NASA Technical Memorandum 83267



# Comparison of Analytical Predictions of Longitudinal Short-Period Pilot-Induced Oscillations With Results From a Simulation Study of the Space Shuttle Orbiter

Donald R. Riley and G. Kimball Miller, Jr.

APRIL 1982



NASA

NASA Technical Memorandum 83267

# Comparison of Analytical Predictions of Longitudinal Short-Period Pilot-Induced Oscillations With Results From a Simulation Study of the Space Shuttle Orbiter

Donald R. Riley and G. Kimball Miller, Jr.
*Langley Research Center*
*Hampton, Virginia*

National Aeronautics
and Space Administration

**Scientific and Technical
Information Branch**

1982

## SUMMARY

An analytical analysis of conditions producing pilot induced oscillations (PIO's) was made for the Space Shuttle orbiter in a landing-approach configuration for the task of nulling the elevation angle of the line of sight to a target vehicle. The analysis yielded a value of PIO frequency and a value for the amount of total-system time delay (pilot + control system) that can be tolerated before instability results. Calculations were performed showing the effect of varying the range to the target and of varying the handling qualities of the orbiter vehicle. Comparisons were made of the analytical predictions and the simulation results obtained using the Langley Visual/Motion Simulator. Similar trends for PIO frequency were obtained for calculated and experimental values due to changes in vehicle handling qualities; however, different trends were noted for changes in target range. Calculated results showed an increase in PIO frequency with a decrease in range, whereas the simulation results were invariant with range. In addition, calculated results showed a reduction in the tolerable amount of time delay with a reduction in range which was supported by the experimental results.

## INTRODUCTION

A recent simulation study (ref. 1) was made using the Langley Visual/Motion Simulator to determine the effect of varying the amount of control-system time delay on the occurrence of pilot induced oscillations (PIO's) and on pilot tracking performance of a Space Shuttle orbiter in a landing-approach configuration. The pilot's task was to track a target airplane that performed a maneuver in altitude only. The target was initially offset laterally so that both orbiter pitch and roll hand-controller inputs were required. PIO's were encountered in both the longitudinal and lateral modes of motion when 250 milliseconds of additional delay were inserted in the simulation.

The purpose of this paper is to present a PIO analytical analysis for the longitudinal short-period motion of the air-to-air tracking task that was simulated in reference 1. The analysis permits determining a value for the PIO frequency and a value of total-system time delay (pilot + control system) beyond which the system goes unstable. Several factors affecting the PIO are examined, such as target range and simulated vehicle handling qualities. Comparisons are made of the simulation results not included in reference 1 and the analytical calculations.

## SYMBOLS

Numerical values are given for some quantities in both the International System of Units (SI) and in U.S. Customary Units for convenience. Measurements and calculations were made in U.S. Customary Units. The effective stability derivatives used herein are referenced to a system of axes with the origin at the vehicle center of gravity.

A,B,C letter designates transfer function listed in table AI of appendix A

a,b,c coefficients of polynomial listed in appendix B

$C_m$ $= \dfrac{M}{\bar{q} S_w \bar{c}}$

$C_{m_q}$ $= \dfrac{\partial C_m}{\partial \dfrac{q\bar{c}}{2V}}$

$C_{m_\alpha}$ $= \dfrac{\partial C_m}{\partial \alpha}$

$C_{m_{\delta e}}$ $= \dfrac{\partial C_m}{\partial \delta_e}$

$C_Z$ $= \dfrac{-L}{\bar{q} S_w}$

$C_{Z_q}$ $= \dfrac{\partial C_Z}{\partial \dfrac{q\bar{c}}{2V}}$

$C_{Z_\alpha}$ $= \dfrac{\partial C_Z}{\partial \alpha}$

$C_{Z_{\delta e}}$ $= \dfrac{\partial C_Z}{\partial \delta_e}$

$\bar{c}$ mean geometric chord, m (ft)

$h$ altitude of orbiter above reference altitude, m (ft)

$\dot{h}$ orbiter altitude rate, m/sec (ft/sec)

$h_t$ target altitude above reference altitude, m (ft)

$I_y$ orbiter moment of inertia about pitch axis, kg-$m^2$ (slug-$ft^2$)

$i$ $= \sqrt{-1}$

$K_p$ pilot gain constant

$L$ lift force, N (lbf)

$L_q$ $= \dfrac{1}{mV} \dfrac{\partial L}{\partial q}$

$L_\alpha$ $= \dfrac{1}{mV} \dfrac{\partial L}{\partial \alpha}$

$L_{\delta_e}$ $= \frac{1}{mV} \frac{\partial L}{\partial \delta_e}$

$\iota_t$ horizontal distance between orbiter c.g. and target c.g. (range for small $\theta_t$), m (ft)

M pitching moment, N-m (lbf-ft)

$M_q$ $= \frac{1}{I_y} \frac{\partial M}{\partial q}$

$M_\alpha$ $= \frac{1}{I_y} \frac{\partial M}{\partial \alpha}$

$M_{\dot{\alpha}}$ $= \frac{1}{I_y} \frac{\partial M}{\partial \dot{\alpha}}$

$M_{\delta_e}$ $= \frac{1}{I_y} \frac{\partial M}{\partial \delta_e}$

m vehicle mass, kg (slugs)

P period of oscillation, sec

q orbiter pitching angular rate, rad/sec

$\bar{q}$ dynamic pressure, $N/m^2$ ($lb/ft^2$)

S Laplace variable

$S_w$ wing area, $m^2$ ($ft^2$)

V orbiter velocity, m/sec (ft/sec) or knots

W orbiter weight, N (lb)

$Y_P$ pilot transfer function

$Y_{PTD}$ combined pilot and time-delay transfer function

$Y_{TD}$ time-delay transfer function

$\alpha$ angle of attack, rad

$\gamma$ flight-path angle, rad

$\Delta$ determinant defined by equation (A3)

$\delta_e$ hand-controller input after scaling, rad

$\varepsilon_v$ vertical tracking error ($h_t$ - h), m (ft)

$\varepsilon_\theta$ line-of-sight angle of pilot (fig. 1), rad

$\zeta$ damping ratio of longitudinal short-period mode

$\theta$ pitch angle, rad or deg

$\theta_t$ angle of target from orbiter measured positive above horizontal (see fig. 1), rad

$\tau$ total time delay ($\tau_e + \tau_a$), sec

$\tau_a$ control-system time delay, sec

$\tau_e$ pilot effective time delay, sec

$\tau_{PIO}$ maximum tolerable time delay before instability results, sec

$\omega$ frequency of oscillation, rad/sec

$\omega_n$ undamped natural frequency of longitudinal short-period mode, rad/sec

$\omega_{PIO}$ frequency of pilot induced oscillation, rad/sec

Abbreviations:

ALT approach and landing tests

c.g. center of gravity

PIO pilot induced oscillation

VMS visual/motion simulator

A dot over a symbol indicates the first derivative with respect to time.

## BACKGROUND

Over the years longitudinal short-period PIO's have been encountered with a number of airplanes. A variety of different factors have been identified as the causative agents in generating these PIO's. Several theories have been advanced to try and predict PIO tendencies. The theory in reference 2 is based on pitch attitude tracking. Reference 3 provides another theory and also gives a bibliography of PIO papers. In reference 3 it is postulated that PIO's are generated by the pilot responding to normal acceleration cues. In the Shuttle orbiter tracking study on the Langley VMS it was believed that the visual task was the main driver in the simulation. Both vehicle pitching and altitude motions were involved. In addition, there were several nonlinear elements in the simulation. Since the theories of references 2 and 3 were not applicable to the task simulated, the present paper presents a PIO analytical analysis tailored specifically to the line-of-sight tracking task studied. The purpose was not to match prediction and experiment exactly, since the simulation involved nonlinear elements and both longitudinal and lateral modes of motion, but instead to indicate the trend linear theory would predict when varying the same parameters as varied in the simulation.

## LINE-OF-SIGHT TRACKING TASK

The six-degree-of-freedom simulator study of reference 1 employed an air-to-air tracking task. For each run, the pilot was to visually track a target airplane as it varied slowly in altitude. Target altitude was driven by a low-frequency cosine wave. For each run only 1/2 cycle of target motion was employed so that the resulting piloting task would approximate a flare to the landing maneuver. For convenience, the orbiter was in a level-flight trim condition at the start of each run. Also, the orbiter was at the same altitude but displaced laterally from the target. A reticle was supplied in the subject's visual field that was held fixed with respect to the orbiter body axes. The pilot's task was to keep the cross hairs on the target both in elevation and azimuth.

The analytical analysis in this paper is concerned only with the orbiter motion in the plane of symmetry. For this situation the pilot's task was to null the elevation line-of-sight angle $\varepsilon_\theta$. The geometry of the situation is depicted in figure 1. In addition to the target aircraft and reticle, the horizon was also displayed to the pilot.

An examination of figure 1 shows the line of sight to be from the orbiter c.g. to the target c.g. This simple geometry is considered herein. The offset of the pilot's eye, forward of the orbiter c.g., and the location of the tail pipe, aft of the target c.g., complicate the geometry. Such arrangements, however, can be considered. The horizon display is of use to the pilot in controlling bank angle, which is, of course, a lateral task. As indicated in figure 1, the pilot's longitudinal task involves only a single input, namely $\varepsilon_\theta$. This geometry yields the multiloop system shown in block diagram form in figure 2.

The various elements of the block diagram are labeled and most are self-explanatory. The block marked time delay represents a transport time delay existing in the control system and was the primary variable in the simulation study of reference 1. One of the basic assumptions made in analyzing the block diagram of figure 2 is that the orbiter speed $V$ remain constant. Another assumption is that the longitudinal distance between orbiter and target also remain constant; that is, $l_t$ is a constant. As a consequence, the dynamics block is reduced to only two degrees of freedom, which is the number required to represent the orbiter longitudinal, open-loop, short-period characteristics.

The pilot's task, as depicted in figure 1 and as modeled in figure 2, is defined strictly as a line-of-sight tracking task. An alternate approach that is sometimes used to model this tracking task is to include an additional pilot-model block in the outer loop (see ref. 4) following the signal $\varepsilon_v \frac{1}{l_t}$ in figure 2. Use of such an additional pilot block was omitted in the present study because of the descriptions given by the astronauts and pilots of the task performed in the simulator. As pointed out in appendix C of reference 1, target aspect cues were seldom used by the subjects. All subjects indicated that keeping the cross hairs on the center of the tail pipe was the tracking goal in the simulation. Also, the subjects indicated that for the longitudinal task the horizon was of little use.

## PIO CONDITION

The PIO condition arises from the circulation of the pilot's input signals in the various loops of the system. For a PIO to exist for the system of figure 2, the use of the low-frequency forcing function $h_t$ is not necessary. Therefore, in a PIO analysis the input $h_t$ can be set equal to zero. Also, in most PIO situations the pilot's input signals seem to have a wave form that closely approximates a sinusoid. This means that an analysis, if the system is linear, need only be concerned with the system frequency response. Finally, the PIO condition is defined to occur at that frequency corresponding to the largest value of time delay that can be tolerated before the system goes unstable.

## ANALYTICAL PROCEDURE

First the characteristic equation for the system of figure 2 was determined. A mathematical model of the pilot was selected and inserted into this equation. By letting $S = i\omega$, the stability boundaries were calculated in terms of two system parameters, pilot gain $K_p$ and total-system time delay $\tau$. From a parameter-plane plot of $K_p$ versus $\tau$, the largest value of $\tau$ before unstable operation and the corresponding value of $K_p$ were extracted. For the analysis herein, these values correspond to the PIO condition. Note that the value of $\omega$ associated with these values of $K_p$ and $\tau$ is labeled the PIO frequency.

## ANALYSIS

The equations of longitudinal motion for the vehicle dynamics block of figure 2 were used to obtain the transfer functions $\frac{\theta}{\delta_e}$ and $\frac{h}{\delta_e}$. Details of the development are given in appendix A.

With $\frac{\theta}{\delta_e}$ and $\frac{h}{\delta_e}$ given, two transfer functions, one representing control-system time delay and the other representing the human pilot, need to be defined. Recall that the transfer function which represents a pure time delay can be written in Laplace notation as

$$Y_{TD} = e^{-\tau_a S} \tag{1}$$

For the pilot model in the inner loop of figure 2, the transfer function selected is

$$Y_p = K_p e^{-\tau_e S} \tag{2}$$

Several choices for a pilot model exist in the literature, from the "synchronous pilot" represented by a simple gain $K_p$ (see ref. 5 and background review in ref. 3), to a very sophisticated model (see ref. 6) that contains lead and lag equalization terms, a time delay, and second-order systems for neuromuscular effects. The pilot model represented by equation (2) discards the lead and lag equalization terms

of the sophisticated model from consideration for the PIO condition; however, it retains the time delay and the lag effects of the neuromuscular system through the use of an effective time delay $\tau_e$.

Since time delay appears in both equations (1) and (2), it was convenient mathematically to combine these two transfer functions as depicted in figure 3(a). Thus

$$Y_{PTD} = K_p e^{-\tau S} \tag{3}$$

where

$$\tau = \tau_e + \tau_a \tag{4}$$

Once the various transfer functions of figure 2 are specified, an analysis of the closed loop can be undertaken and the system characteristic equation can be derived. Details of the derivation are presented in appendix B. The characteristic equation thus obtained can be written as

$$S^2 \Delta + Y_{PTD}\left(AS + \frac{VB}{l_t}\right) = 0 \tag{5}$$

where A, B, and $\Delta$ are defined in table AI. Substituting equation (3) into equation (5) yields

$$S^2 \Delta + K_p e^{-\tau S}\left(AS + \frac{VB}{l_t}\right) = 0 \tag{6}$$

This equation involves the two unknown parameters $K_p$ and $\tau$. To obtain stability boundaries, substitute $S = i\omega$ into equation (6) and determine the values for $K_p$ and $\tau$ which satisfy the resulting equation.

In solving an expression such as equation (6) that involves two unknown parameters, the general technique is to rewrite the single equation as two equations. One of the new equations deals with the real part of the original expression and the other deals with the imaginary part. These two equations with two unknowns can then be solved simultaneously to determine values of the unknown parameters. However, in the particular case of equation (6), a different approach is necessary since it involves an exponential term. This different approach solves for the amplitude and phase angle of $Y_{PTD}$. Evaluation of $K_p$ is then possible since it is associated only with the amplitude, and similarly, evaluation of $\tau$ is possible since it is associated only with the phase angle. (See ref. 7.)

An illustrative parameter-plane plot of $K_p$ versus $\tau$ is given in the sketch in figure 3(b). The curve is a stability boundary that divides the parameter plane into stable and unstable regions. In the sketch the maximum value of $\tau$ is labeled

as the PIO condition. This is the largest value of time delay that can be tolerated before the system goes unstable. With this value of $\tau$ there exists a single corresponding value of $K_p$. Associated with these two values is a frequency called the PIO frequency ($\omega_{PIO}$).

In figure 3(c) additional detail is presented that helps illustrate the reasoning behind the selection of the PIO condition. Recall that $\tau$ is the sum of two delays, $\tau_e$ and $\tau_a$. Since the pilot's effective time delay $\tau_e$ is unchanging, and therefore a constant, there must exist an inaccessible region in the parameter plane as shown in the sketch. That is, $\tau = \tau_e$ is the minimum possible delay value. Of course, if $\tau = \tau_e$ the amount of control-system time delay $\tau_a$ is zero. The range of $K_p$ represented by a vertical line at this value of delay and contained within the stability boundary is quite large. From an examination of figure 3(c), it is apparent that adding an increment of control-system time delay $\tau_a$ results in a decrease in the range of possible pilot gain for stable system operation. Continuing to increase $\tau_a$ constrains the stable range of pilot gain even more. Finally, there exists a single value of delay $\tau_{PIO}$ beyond which the system is unstable no matter what the value of pilot gain. Thus, it is apparent that for any value of $\tau$ less than $\tau_{PIO}$, the pilot has the ability if he finds that he is operating in an unstable region of the parameter plane to achieve stable operation by simply altering his gain. For the PIO condition, the pilot can no longer affect system stability by adjusting his gain.

It is, of course, recognized that any point along the boundary defines a stability situation that can be labeled as a PIO condition. The use of rationale other than that just described could lead to selecting any number of different points along the boundary curve as PIO conditions. As a consequence, different values of pilot gain, time delay, and frequency would result. For this paper, constraining the pilot's control action in the manner described previously seems an appropriate choice for the tracking task simulated.

It is of interest to note that in the simulation study of reference 1, the hand-controller characteristics were nonlinear. For this analysis, the hand-controller characteristics are assumed linear. Controller characteristics enter the pilot transfer function as a single constant gain and thus are contained in $K_p$.

## CASES CONSIDERED

The cases calculated were chosen to provide a range of values that would encompass the test conditions of a set of simulator runs obtained as a sequel to the study of reference 1. The analytical calculations used the stability derivatives and physical characteristics given in table I. These values are identical to those used in reference 1 for the Shuttle orbiter. Table II provides expressions for converting the nondimensional derivatives of table I to the dimensional form for use in the mathematical development herein.

The cases calculated are concerned with examining the effect of range and the effect of changing vehicle handling qualities. Calculations were performed for six equally spaced values of range, from 30.48 m (100 ft) to 182.88 m (600 ft), for each different set of parameter values considered. Vehicle handling qualities were varied by using the four different sets of parameter values given in table III. Three sets of dimensional parameters were obtained by simply increasing or decreasing the orbiter speed from the value used in reference 1 (basic case). The remaining set was obtained by changing the single stability derivative $C_{Z_\alpha}$ of the basic case.

## RESULTS AND DISCUSSION

### General Remarks

The analytical development presented herein provides the following two numerical results:

1. A value for the PIO frequency

2. A value for control-system time delay beyond which the closed-loop system goes unstable

The calculated results for these two entities are discussed in the next section entitled "Analytical Results." The effects of range and changing orbiter handling qualities are covered briefly. The purpose of the calculations was to provide values that correspond to simulator supplemental test data. Explanations and the reason for performing the supplemental simulator study are presented in the "Experimental Results" section. A comparison section discusses the trends obtained from theory and from experiment.

### Analytical Results

Calculations were performed to determine the values of pilot gain $K_p$ and time delay $\tau$ as a function of frequency for six different values of range between orbiter and target for each of the four different handling-quality cases given in table III. Values of range $\imath_t$ from 30.48 m (100 ft) to 182.88 m (600 ft) were used. Parameter-plane plots of $K_p$ versus $\tau$ were constructed at each value of range and the PIO conditions were determined. Most of the parameter-plane plots were as sketched in figures 3 and 4(a). For the shorter ranges, however, a loop appeared as shown in figure 4(b) that enlarged in size as range was reduced. For these situations the PIO condition occurred at the loop closure point. The PIO conditions obtained from all of the parameter-plane plots are given in figures 5 and 6 showing PIO frequency $\omega_{PIO}$ and time delay $\tau_{PIO}$ as a function of range between orbiter and target.

All of the curves shown in figures 5 and 6 indicate that $\omega_{PIO}$ increased with a reduction in range. In addition, as range was reduced the amount of time delay $\tau_{PIO}$ that could be tolerated in the system before instability resulted was also reduced. As a consequence, these results point out the dilemma facing a pilot performing the task of closing on a target. It is readily apparent that as range is reduced, some value of range will be encountered at which a PIO will occur and below which the pilot-vehicle system will go unstable.

Changing vehicle handling qualities is accomplished herein in two different ways. One way is by changing the orbiter speed and the other way is by changing a single derivative $C_{Z_\alpha}$. Both ways were used in the supplemental simulator tests. The values of $V$ and $C_{Z_\alpha}$ used here are the same as those used in the simulator runs. Results for the effect of handling qualities on PIO conditions of frequency $\omega_{PIO}$ and time delay $\tau_{PIO}$ can be assessed using the different curves in figures 5 and 6. Increasing either speed or the magnitude of $C_{Z_\alpha}$ improves the vehicle

handling qualities. At any given value of range, an increase in $V$ or the magnitude of $C_{Z_\alpha}$ increases $\omega_{PIO}$ and reduces $\tau_{PIO}$.

It is worth noting that the total amount of time delay in the system $\tau_{PIO}$ is used as the ordinate in figures 5 and 6. From equation (4) recall that the total time-delay value consists of the sum of two parts, one part due to the pilot $\tau_e$ and the other part due to the control system $\tau_a$. To ascertain the amount of time delay at the PIO condition due to the control system requires that an estimate be made of the pilot delay term $\tau_e$ and the difference determined. A typical value of $\tau_e$ of about 200 msec is believed to correspond to the normal experience of a pilot performing a conventional tracking task. A value of $\tau_e$ of 100 msec can be considered as a lower limit or bound of pilot effective time delay when the pilot is represented by the simple transfer function of equation (2) and when he is pushed to his operating limit. Such a case might occur during a PIO. Simply reducing the ordinate values of $\tau_{PIO}$ in figures 5 and 6 by a value of $\tau_e$ of 100 msec provides the largest values of control-system time delay $\tau_a$ that can be tolerated before the pilot-vehicle system becomes unstable.

## Experimental Results

The simulator study of reference 1 using two astronauts and two research pilots as test subjects gave periods for the longitudinal PIO's of about 5 sec for all test subjects. The period of the PIO obtained on landing number 5 of the Shuttle orbiter at Dryden Flight Center was about 2.5 sec. Because of this difference, a few additional tests were made in the Langley Visual/Motion Simulator using one of the research pilots in the original study to see if a 2.5-sec period could be obtained with the simulator.

In the original simulation, the PIO's were found to occur near the end of the run. For those tests the range between the target vehicle and the orbiter was varied linearly with time. Initial range was 182.88 m (600 ft) and final range was 91.44 m (300 ft). Run time was 60 sec. At run termination the target wing span in the visual scene matched the width of the horizontal bar of the reticle. This scheme was used to induce the pilot to increase his gains as he normally does during the landing flare. Because the PIO's occurred at the closer ranges, some supplemental runs holding range constant were made at even closer ranges. Runs were made at 91.44 m (300 ft), 60.96 m (200 ft), and 30.48 m (100 ft) to determine the effect of range on PIO period. The runs were made with various amounts of time delay present. PIO's did not occur for all of the runs made; however, sufficient oscillations occurred in the $\alpha$ and $\theta$ time-history traces to determine a value for the period due to control inputs. The results of these tests indicate that the period of the oscillatory motions was invariant with range. Some additional runs were then made for different vehicle speeds. The original simulation setup was for a 300-knot (500 ft/sec) Shuttle orbiter. Two additional speeds were tested with one greater and one less than the original 300-knot speed. At each speed several runs were made at the different ranges. Figure 7 presents the results of these tests. Note that changing speed changes the handling qualities of the vehicle as shown in figure 8 (ref. 8). The results show that for the higher speed configurations (better handling qualities), the period of the oscillatory motions was reduced to about 3 sec. The period, however, remained invariant with range for the different speeds.

Increasing speed affects both the longitudinal and lateral handling characteristics. Earlier tests have shown that an improvement in one channel usually results in an improvement in the other channel. To eliminate the possible influence of an

easier lateral task, one single derivative $C_{Z_\alpha}$ was changed from -3.45 to -6.90 for the same 300-knot speed condition to give only a change in vehicle longitudinal characteristics. Several runs were made at the same three ranges. The results are shown in figure 9. The data for the Shuttle vehicle from figure 7 are shown for comparison. Periods of the oscillatory motions in $\alpha$ and $\theta$ were 3 sec for the modified configuration. Figure 10 (ref. 8) locates this modified configuration on the handling qualities chart.

Figures 11 and 12 show the time-history records of several of the runs made. Note that in figure 11 the pilot tried to keep his gains high and, consequently, at about 45 sec the motion base drive signals exceeded some preset limitations and the motion base automatically reset to the neutral position. In figure 12 the pilot simply stopped making inputs at about 45 sec. In both figures, $\varepsilon_\theta$ is the line-of-sight angle and $\delta_e$ is the hand-controller input behind the quadratic shaper that goes directly into the equations of motion.

The basic conclusions from these supplemental tests were that (1) the PIO frequency is invariant with range, (2) PIO frequency increases with an increase in speed (improved handling qualities), and (3) PIO frequency increases with an increase in $C_{Z_\alpha}$ (improved handling qualities). It is important to note that the main purpose of these supplemental tests was to establish the frequency of the PIO. No effort was made to assess the amount of control-system time delay necessary for PIO to occur at any given test condition of range and speed.

It should be pointed out that the target vertical movement during the run and the orbiter lateral offset at run initiation were arbitrarily reduced as the range $l_t$ was reduced. These changes were introduced in order that the elevation and azimuth visual angles presented to the subject during the run remained at about the same order of magnitude. Also, for the data presented herein, the offset of the pilot's eye from the orbiter c.g. was eliminated. Finally, in performing the supplemental tests the same amount of time delay was inserted in both the pitch and roll control channels immediately following the pilot's control input signals. The set of time-delay values used were 0, 4, 8, and 12 units of time delay as used in reference 1 where each unit represents the update interval of the digital computer used. (Each unit represents 31.25 msec.) Each of these values has been increased by 50 msec to account for the delay present in the digital computer from input to output and for the delay present in the visual scene generation equipment. (See ref. 1.) These are the values listed as $\tau_a$ in figures 7 to 12.

## Comparison of Results

A comparison of experimental results and analytical predictions for the PIO condition is given in figure 13. Separate comparisons are presented for each of the four different handling-quality cases tested. An examination of the four frequency plots shows, as pointed out earlier in the text, the invariance with range of the experimental data and the increase in frequency with decreasing range of the analytical results. Of additional interest is the fact that the predictions give a larger value of PIO frequency than was obtained experimentally for all test conditions.

Comparisons of the PIO condition for time delay are also given in figure 13. The total value of time delay $\tau_{PIO}$ is presented. In order to make the comparisons, a value of $\tau_e$ had to be added to the experimental delay values used for the

simulator tests. A value for $\tau_e$ of 100 msec was used. Also, the simulator had about a 50-msec delay due to the digital computer and visual display employed. (See previous section and also ref. 1.) Therefore, the minimum value of $\tau$ that could be tested was about 150 msec. Figure 13 shows several tests performed at this condition. In examining the figure it is interesting to note that at the closest range tested even this minimum value of time delay exceeded the values of the calculated curve. In fact, for most tests in the simulator the values of time delay used exceeded those predicated as the PIO condition by the analytical analysis. Of course at the time the tests were made the analysis had not been initiated. Notice that shading of the time-delay symbols is used to distinguish those cases in which PIO's occurred. When the experimental test points lie below and to the right of the boundary no PIO's occurred. In the region of the boundary when the PIO's occurred they occurred near the end of the simulation run. When the experimental points were far to the left or above the curve a definite instability occurred early in the run and the time-history traces of the PIO were very erratic throughout. For such circumstances the analytical analysis indicated that an unstable situation existed. What occurred in reality was that the pilot altered his tracking task and no longer tracked the target as postulated in the mathematical analysis.

It is worth pointing out that the research pilot used for the supplemental tests and all of the test subjects of reference 1 indicated that the task in the simulator was a line-of-sight tracking task as modeled herein. It is possible, however, by altering the model to obtain theoretical values for $\omega_{PIO}$ that are invariant with range. This can be accomplished by including an additional pilot gain constant in the outer loop of figure 2 with $\varepsilon_v \frac{1}{\iota_t}$ as the input. It is readily apparent that adjustment of the value of this additional pilot gain to offset the effects of changes in $1/\iota_t$ would provide results invariant with range. Note that this is equivalent to subjects changing their aim point to other locations inside the tailpipe area rather than the center. Acceptance of an area as the aim point is believed to be what the pilot used as a practical goal in performing the task in the simulator at the closer ranges. The subject comments in appendix C of reference 1 support this altering of the tracking goal at the closer ranges.

To facilitate examining the effect of vehicle handling qualities on frequency, figure 14 presents a comparison of analytical predictions and experimental results for a single value of range $\iota_t$ of 91.44 m (300 ft). The differences in magnitude between experimental and calculated values could be expected from the comparisons in figure 13. The trends of the results, however, with improving handling qualities either by increasing the vehicle's speed or by changing the single derivative $C_{Z_\alpha}$ were comparable.

It is important to note that there are other possible reasons for differences existing between the simulation results and the analytical predictions, such as

1. The simulation involved six degrees of freedom and the tracking task required the pilot to make both pitch and roll control inputs for task accomplishment. For the supplemental tests the same amount of time delay was inserted following the pitch and roll control input signals from the hand controller. When the pilot experienced control difficulties longitudinally he nearly always had difficulties laterally. Thus, the experiment involves a multi-axis control task whereas the theory is for a single-axis task.

2. Motion cues were present in the simulator and not accounted for in the theory.

3. A quadratic shaping circuit modifying the hand-controller output was present in the simulation and not in the theory.

4. Subject awareness of potential resetting of the motion base to the neutral position because of overly aggressive control action could have resulted in an experimental task at the closer ranges different from the theory.

There is one other comparison of PIO frequency that needs to be considered, and that is a comparison between the PIO periods obtained in the simulation of the basic case ($P \approx 5$ sec) and in the full-scale orbiter flight tests at Edwards Air Force Base ($P \approx 2.5$ sec). One possible reason for the difference is that the orbiter aerodynamics at the time of the PIO were not identical. The PIO of free flight number 5 occurred just prior to touchdown. For this condition the vehicle was in ground effect. For the simulation, the orbiter was modeled at an altitude of about 457 m (1500 ft). Thus, some differences exist in the orbiter aerodynamic characteristics for these two cases which could be expected to affect the PIO periods. In addition, the piloting tasks were not the same. For the flight tests, the pilot was also concerned with modulating the flight velocity, executing a landing flare, arresting the sink rate, and achieving the desired attitude for touchdown. These additional concerns were missing in the simulation; nevertheless, it should be noted that the pilot's task in free flight number 5 was to land at a particular spot on the runway. Thus, as the orbiter proceeded along the glide slope the pilot was performing a tracking task to achieve the touchdown point that is similar to the task modeled analytically herein. The fact that a PIO occurred for the Shuttle orbiter on free flight number 5 should not be too surprising since the analysis herein shows that for a line-of-sight tracking task the amount of time delay that can be tolerated in the system for stable operation decreases as range to the target decreases.

## CONCLUDING REMARKS

An analytical analysis of conditions producing pilot induced oscillations (PIO's) was made for a Shuttle orbiter configuration for the task of nulling the elevation angle of the line of sight to a target vehicle. The analysis yielded a value of PIO frequency and a value for the amount of total-system time delay that can be tolerated before instability results. Calculations were performed showing the effect of varying the range to the target and of varying the handling qualities of the orbiter vehicle. Comparisons of the analytical predictions were made with results from a six-degree-of-freedom simulation using the Langley Visual/Motion Simulator.

Results of the analytical analysis indicated an increase in PIO frequency with a decrease in range, whereas the simulation results were invariant with range for the ranges tested. Predicted values of total-system time delay that could be tolerated before PIO occurs decreased with a decrease in range. For both calculated and experimental results, improving the vehicle handling qualities either by increasing the vehicle speed or by increasing the magnitude of the single stability derivative $C_{Z_\alpha}$ increased the frequency and reduced the tolerable value of time delay.

The analytical analysis presented herein was made for the purpose of indicating what linear theory would predict for a visual line-of-sight tracking task. It was

felt that the results supplement the simulator data and perhaps offer some explanation for the variations obtained. It is recognized that a number of factors other than time delay can result in PIO's, such as control-system nonlinearities, rate limiting of control surfaces, acceleration effects, and others. This study also indicates that PIO can be task dependent. Thus, the results are not believed to be directly applicable to analyzing the longitudinal PIO obtained in free flight number 5 of the approach and landing tests (ALT) since the piloting tasks are not the same. It is felt, however, that a similar trend toward instability with decreasing range for a line-of-sight tracking task would apply.

Langley Research Center
National Aeronautics and Space Administration
Hampton, VA 23665
March 19, 1982

## APPENDIX A

## EQUATIONS OF MOTION, SHORT-PERIOD CHARACTERISTICS, AND OPEN-LOOP TRANSFER FUNCTIONS

The standard linearized longitudinal perturbation equations of motion are used for this mathematical development. They are further simplified by the following assumptions:

1. Constant airspeed

2. Initial condition is straight and level flight

3. Stability derivative $M_{\dot{\alpha}}$ is neglected

Under these conditions the equations of motion, written in Laplace notation are

$$(S + L_\alpha)\alpha + (L_q - 1)q = -L_{\delta_e}\delta_e \tag{A1}$$

$$(-M_\alpha)\alpha + (S - M_q)q = M_{\delta_e}\delta_e \tag{A2}$$

The longitudinal short-period mode characteristics can be easily obtained from equations (A1) and (A2). For convenience

$$\Delta = \begin{vmatrix} (S + L_\alpha) & (L_q - 1) \\ (-M_\alpha) & (S - M_q) \end{vmatrix} \tag{A3}$$

The characteristic equation can be obtained by expanding the determinant in equation (A3) and setting the result equal to zero. Thus

$$S^2 + (L_\alpha - M_q)S + M_\alpha(L_q - 1) - L_\alpha M_q = 0 \tag{A4}$$

From this

$$\omega_n^2 = M_\alpha(L_q - 1) - L_\alpha M_q \tag{A5}$$

$$2\zeta\omega_n = L_\alpha - M_q \tag{A6}$$

and

$$\zeta = \frac{L_\alpha - M_{\dot{q}}}{2\left[M_\alpha(L_q - 1) - L_\alpha M_q\right]^{1/2}} \tag{A7}$$

Using equations (A1) and (A2) the open-loop transfer functions $\frac{q}{\delta_e}$, $\frac{\theta}{\delta_e}$, and $\frac{\alpha}{\delta_e}$ can be obtained directly as

$$\frac{q}{\delta_e} = \frac{\begin{vmatrix} (S + L_\alpha) & \left(-L_{\delta_e}\right) \\ (-M_\alpha) & \left(M_{\delta_e}\right) \end{vmatrix}}{\begin{vmatrix} (S + L_\alpha) & (L_q - 1) \\ (-M_\alpha) & (S - M_q) \end{vmatrix}} \tag{A8}$$

$$\frac{\theta}{\delta_e} = \frac{1}{S}\frac{q}{\delta_e} \tag{A9}$$

$$\frac{\alpha}{\delta_e} = \frac{\begin{vmatrix} \left(-L_{\delta_e}\right) & (L_q - 1) \\ \left(M_{\delta_e}\right) & (S - M_q) \end{vmatrix}}{\begin{vmatrix} (S + L_\alpha) & (L_q - 1) \\ (-M_\alpha) & (S - M_q) \end{vmatrix}} \tag{A10}$$

Table AI lists these transfer functions in expanded form.

The altitude transfer function can be obtained by recalling (see fig. 2)

$$\gamma = \theta - \alpha \tag{A11}$$

and

$$\gamma = \frac{\dot{h}}{V} \tag{A12}$$

Combining equations (A11) and (A12) yields

$$\frac{\dot{h}}{V} = \left(\frac{\theta}{\delta_e} - \frac{\alpha}{\delta_e}\right)\delta_e \tag{A13}$$

Rearranging equation (A13) gives

$$\frac{\dot{h}}{\delta_e} = V\left(\frac{\theta}{\delta_e} - \frac{\alpha}{\delta_e}\right) \tag{A14}$$

and finally

$$\frac{h}{\delta_e} = \frac{V}{s}\left(\frac{\theta}{\delta_e} - \frac{\alpha}{\delta_e}\right) \tag{A15}$$

With the appropriate substitution, equations (A14) and (A15) are expanded and given in table AI.

APPENDIX A

TABLE AI.- OPEN-LOOP TRANSFER FUNCTIONS

| Symbol | Literal form |
|---|---|
| $\frac{q}{\delta_e}$ | $\frac{A}{\Delta}$ |
| $\frac{\theta}{\delta_e}$ | $\frac{A}{S\ \Delta}$ |
| $\frac{\alpha}{\delta_e}$ | $\frac{C}{\Delta}$ |
| $\frac{\dot{h}}{\delta_e}$ | $\frac{VB}{S\ \Delta}$ |
| $\frac{h}{\delta_e}$ | $\frac{VB}{S^2\ \Delta}$ |
| $\Delta$ | $S^2 + (L_\alpha - M_q)S + \left[M_\alpha(L_q - 1) - L_\alpha M_q\right]$ |
| A | $M_{\delta_e} S + \left(M_{\delta_e} L_\alpha - M_\alpha L_{\delta_e}\right)$ |
| B | $L_{\delta_e} S^2 + \left[M_{\delta_e} - L_{\delta_e} M_q + M_{\delta_e}(L_q - 1)\right] S + \left(M_{\delta_e} L_\alpha - M_\alpha L_{\delta_e}\right)$ |
| C | $-L_{\delta_e} S + \left[L_{\delta_e} M_q - M_{\delta_e}(L_q - 1)\right]$ |

## APPENDIX B

## CLOSED-LOOP ANALYSIS

The following expressions were developed using the block diagrams of figures 2 and 3(a). From the diagrams

$$\varepsilon_v = h_t - h \tag{B1}$$

Rewriting h as

$$h = \left(\frac{h}{\varepsilon_v}\right)\varepsilon_v \tag{B2}$$

and inserting into equation (B1) yields

$$\frac{h}{\left(\frac{h}{\varepsilon_v}\right)} + h = h_t \tag{B3}$$

Rearranging gives

$$\frac{h}{h_t} = \frac{\left(\frac{h}{\varepsilon_v}\right)}{1 + \left(\frac{h}{\varepsilon_v}\right)} \tag{B4}$$

The characteristic equation for the system of figure 2 can be obtained by setting the denominator of equation (B4) equal to zero. Thus

$$1 + \left(\frac{h}{\varepsilon_v}\right) = 0 \tag{B5}$$

Rewrite equation (B5) as

$$1 + \left(\frac{h}{\theta_t}\right)\left(\frac{\theta_t}{\varepsilon_v}\right) = 0 \tag{B6}$$

Note that

$$\frac{\theta_t}{\varepsilon_v} = \frac{1}{\iota_t} \tag{B7}$$

Substituting this identity into equation (B7) and rewriting gives

$$1 + \frac{1}{\iota_t}\frac{h}{\varepsilon_\theta}\frac{\varepsilon_\theta}{\theta_t} = 0 \tag{B8}$$

but

$$\frac{\varepsilon_\theta}{\theta_t} = \frac{1}{1 + Y_\theta} \tag{B9}$$

where

$$Y_\theta = \left(\frac{\theta}{\delta_e}\right)\left(\frac{\delta_e}{\varepsilon_\theta}\right) \tag{B10}$$

Substituting equation (B9) into equation (B8) and rearranging gives

$$1 + Y_\theta + \frac{1}{\iota_t}\left(\frac{h}{\varepsilon_\theta}\right) = 0 \tag{B11}$$

Now using appendix A and figure 3(a) rewrite equation (B10) as

$$Y_\theta = \frac{A}{S\ \Delta}\, Y_{PTD} \tag{B12}$$

Similarly

$$\frac{h}{\varepsilon_\theta} = \left(\frac{h}{\delta_e}\right)\left(\frac{\delta_e}{\varepsilon_\theta}\right) \tag{B13}$$

and

$$\frac{h}{\varepsilon_\theta} = \frac{VB}{S^2\ \Delta}\ Y_{PTD} \tag{B14}$$

Inserting equations (B12) and (B14) into equation (B11) yields

$$1 + \frac{A}{S\ \Delta}\ Y_{PTD} + \frac{1}{\iota_t}\ \frac{VB}{S^2\ \Delta}\ Y_{PTD} = 0 \tag{B15}$$

Combining terms yields

$$S^2\ \Delta + Y_{PTD}\left(AS + \frac{VB}{\iota_t}\right) = 0 \tag{B16}$$

Substituting for A and B from table AI and expanding yields

$$S^2\ \Delta + Y_{PTD}\left(aS^2 + bS + c\right) = 0 \tag{B17}$$

The coefficients a, b, and c are given in the following table and the expression for $\Delta$ is given in table AI:

| Symbol | Expression |
|---|---|
| a | $\frac{V}{\iota_t} L_{\delta_e} + M_{\delta_e}$ |
| b | $M_{\delta_e} L_\alpha - M_\alpha L_{\delta_e} + \frac{V}{\iota_t}\left[M_{\delta_e} - L_{\delta_e} M_q + M_{\delta_e}(L_q - 1)\right]$ |
| c | $\frac{V}{\iota_t}\left(M_{\delta_e} L_\alpha - M_\alpha L_{\delta_e}\right)$ |

Equation (B17) was used to compute the parameter-plane curves presented herein after first rearranging the equation to solve for $Y_{PTD}$ and then substituting $K_p e^{-\tau S}$ for $Y_{PTD}$ as indicated in the text.

## REFERENCES


1. Riley, Donald R.; and Miller, G. Kimball, Jr.: Simulator Study of the Effect of Control-System Time Delays on the Occurrence of Pilot-Induced Oscillations and on Pilot Tracking Performance With a Space-Shuttle-Orbiter Configuration. NASA TP-1588, 1980.

2. Neal, T. Peter; and Smith, Rogers E.: An In-Flight Investigation To Develop Control System Design Criteria for Fighter Airplanes. Tech. Rep. AFFDL-TR-70-74, Vols. I and II, U.S. Air Force, Dec. 1970. (Available from DTIC as AD 880 426 and AD 880 252.)

3. Smith, Ralph H.: A Theory for Longitudinal Short-Period Pilot Induced Oscillations. AFFDL-TR-77-57, U.S. Air Force, June 1977. (Available from DTIC as AD A056 982.)

4. Adams, James J.; and Hatch, Howard G., Jr.: An Approach to the Determination of Aircraft Handling Qualities by Using Pilot Transfer Functions. NASA TN D-6104, 1971.

5. Ashkenas, Irving L.; Jex, Henry R.; and McRuer, Duane T.: Pilot-Induced Oscillations: Their Cause and Analysis. Norair Rep. NOR-64-143 (Rep. STI TR-239-2), Northrop Corp., June 20, 1964.

6. Parker, James F., Jr.; and West, Vita R., eds.: Bioastronautics Data Book, Second ed. NASA SP-3006, 1973, pp. 754-755.

7. Loo, S. G.: Stability of Linear Stationary Systems With Time Delay. Int. J. Contr., vol. 9, no. 1, 1969, pp. 103-109.

8. Etkin, Bernard: Dynamics of Atmospheric Flight. John Wiley & Sons, Inc., c.1972, p. 513.

TABLE I.- STABILITY DERIVATIVES AND PHYSICAL CHARACTERISTICS

[Used herein and in the simulation of reference 1]

| Stability derivatives |
|---|
| $C_{Z_\alpha} = -3.4490$ |
| $C_{Z_q} = -17.5013$ |
| $C_{Z_{\delta e}} = 0.5744$ |
| $C_{m_\alpha} = -0.0253$ |
| $C_{m_q} = -16.4431$ |
| $C_{m_{\delta e}} = 0.2922$ |
| **Physical characteristics** |
| $W = 817\ 761.0617$ N (183 840 lb) |
| $S_w = 249.9092\ m^2$ (2690 $ft^2$) |
| $\bar{c} = 12.0602$ m (39.5675 ft) |
| $I_y = 8\ 729\ 397.232$ kg-$m^2$ (6 438 473 slug-$ft^2$) |

TABLE II.- DIMENSIONAL-DERIVATIVE CONVERSION FORMULA AND EQUATIONS FOR VEHICLE OPEN-LOOP LONGITUDINAL SHORT-PERIOD CHARACTERISTICS

$$L_\alpha = \frac{-\bar{q}S_w}{mV} C_{Z_\alpha}$$

$$L_q = \frac{-\bar{q}S_w}{mV} C_{Z_q} \frac{\bar{c}}{2V}$$

$$L_{\delta_e} = \frac{-\bar{q}S_w}{mV} C_{Z_{\delta e}}$$

$$M_\alpha = \frac{\bar{q}S_w\bar{c}}{I_y} C_{m_\alpha}$$

$$M_q = \frac{\bar{q}S_w\bar{c}}{I_y} C_{m_q} \frac{\bar{c}}{2V}$$

$$M_{\delta_e} = \frac{\bar{q}S_w\bar{c}}{I_y} C_{m_{\delta e}}$$

$$\omega_n^2 = -(M_\alpha + L_\alpha M_q - M_\alpha L_q)$$

$$2\zeta\omega_n = L_\alpha - M_q$$

TABLE III.- VALUES OF DIMENSIONAL DERIVATIVES AND VEHICLE OPEN-LOOP LONGITUDINAL SHORT-PERIOD CHARACTERISTICS

| Parameter | Low speed | Basic case | High speed | Modified basic case[a] |
|---|---|---|---|---|
| V, m/sec | 86.8680 | 152.4000 | 217.9320 | 152.4000 |
| V, ft/sec | 285 | 500 | 715 | 500 |
| V, knots (approx.) | 170 | 300 | 430 | 300 |
| $\bar{q}$, $N/m^2$ | 4624.1077 | 14 232.4067 | 29 103.8472 | 14 232.4067 |
| $\bar{q}$, $lb/ft^2$ | 96.5765 | 297.2500 | 607.8465 | 297.2500 |
| $L_\alpha$ | .5508 | .9664 | 1.3819 | 1.8727 |
| $L_q$ | .1940 | .1940 | .1940 | .1940 |
| $L_{\delta_e}$ | -.0917 | -.1609 | -.2301 | -.1609 |
| $M_\alpha$ | -.0399 | -.1229 | -.2512 | -.1229 |
| $M_q$ | -1.8176 | -3.1887 | -4.5598 | -3.1887 |
| $M_{\delta_e}$ | .4665 | 1.4359 | 2.9363 | 1.4359 |
| $\omega_n^2$ | 1.0333 | 3.1805 | 6.5037 | 6.2619 |
| $\omega_n$ | 1.0165 | 1.7834 | 2.5502 | 2.5024 |
| $\zeta$ | 1.1649 | 1.1649 | 1.1649 | 1.0113 |
| $2\zeta\omega_n$ | 2.3682 | 4.1551 | 5.9417 | 5.0614 |

[a]Changed only $C_{Z_\alpha}$ to -6.90 from -3.45 of basic case.

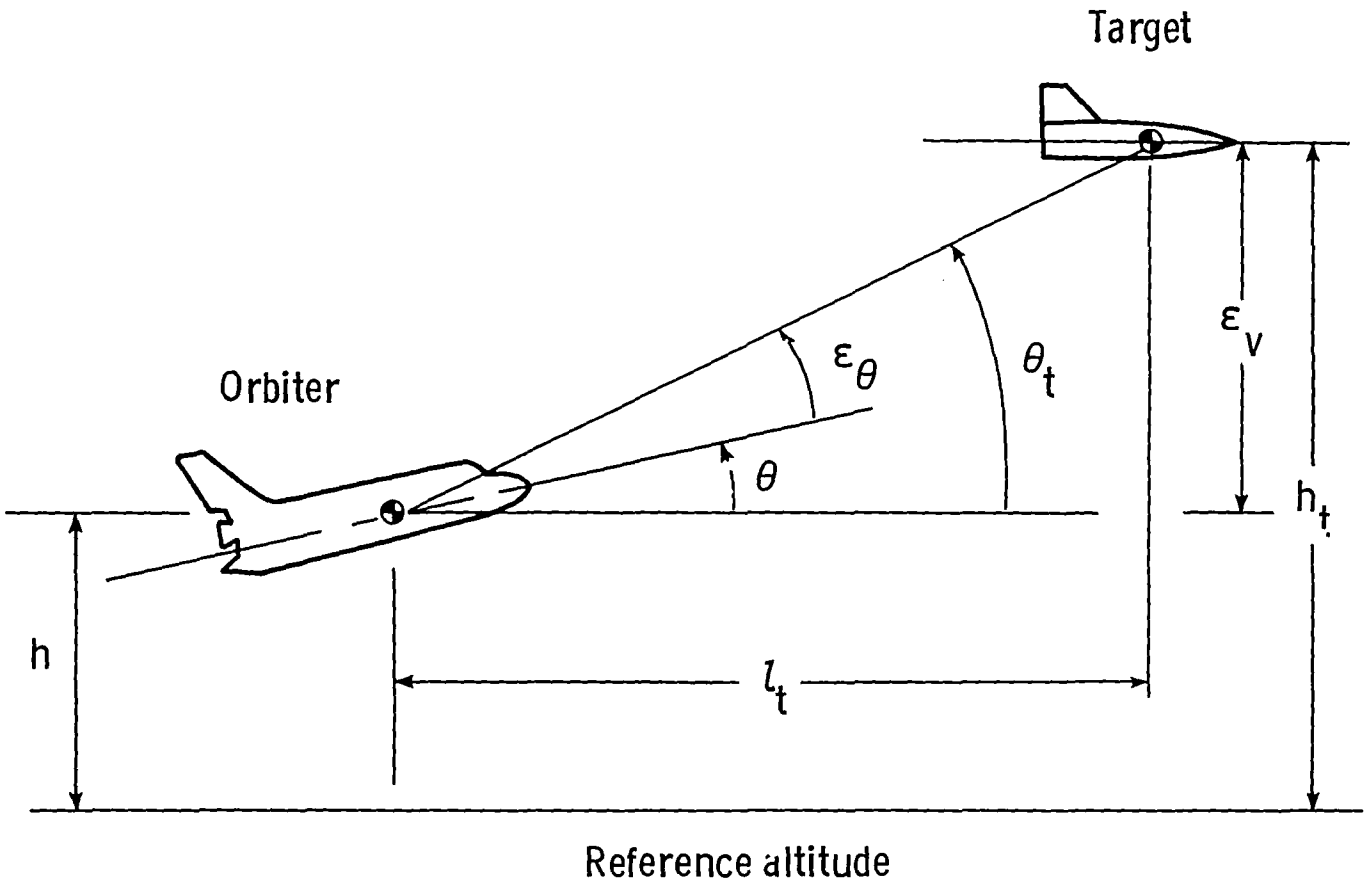


Figure 1.- Tracking task geometry. (Positive values of variables are shown.)

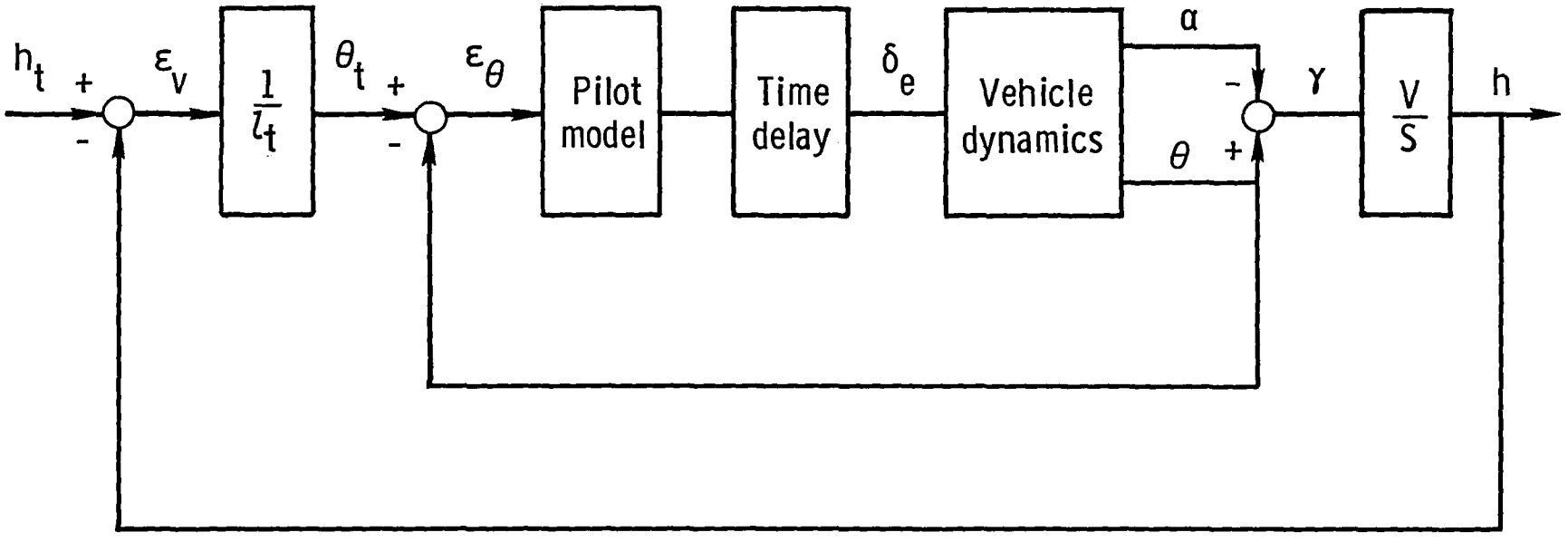


Figure 2.- Block diagram of line-of-sight tracking task.

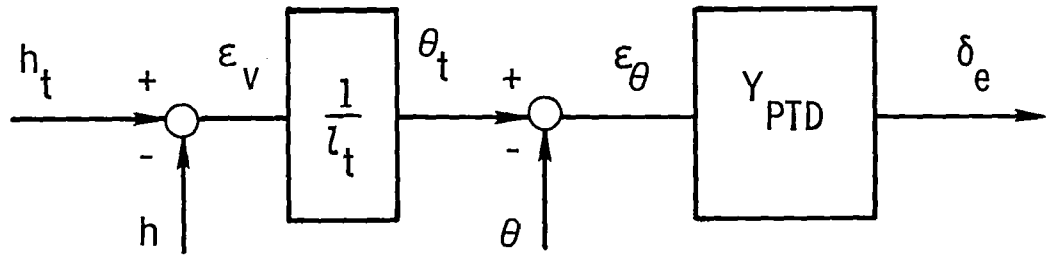


(a) Section of closed-loop system.

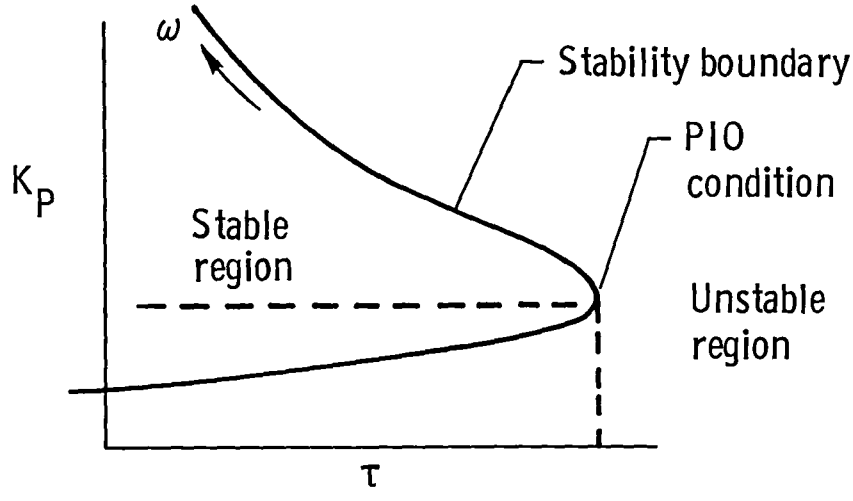


(b) PIO condition in parameter plane.

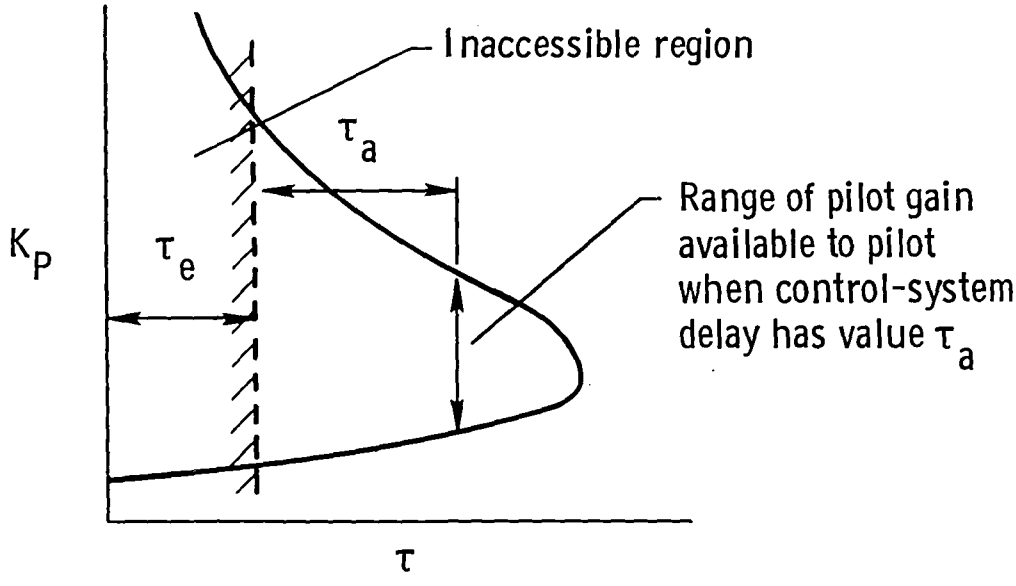


(c) Arbitrary location in parameter plane.

Figure 3.- Closed-loop analysis sketches.

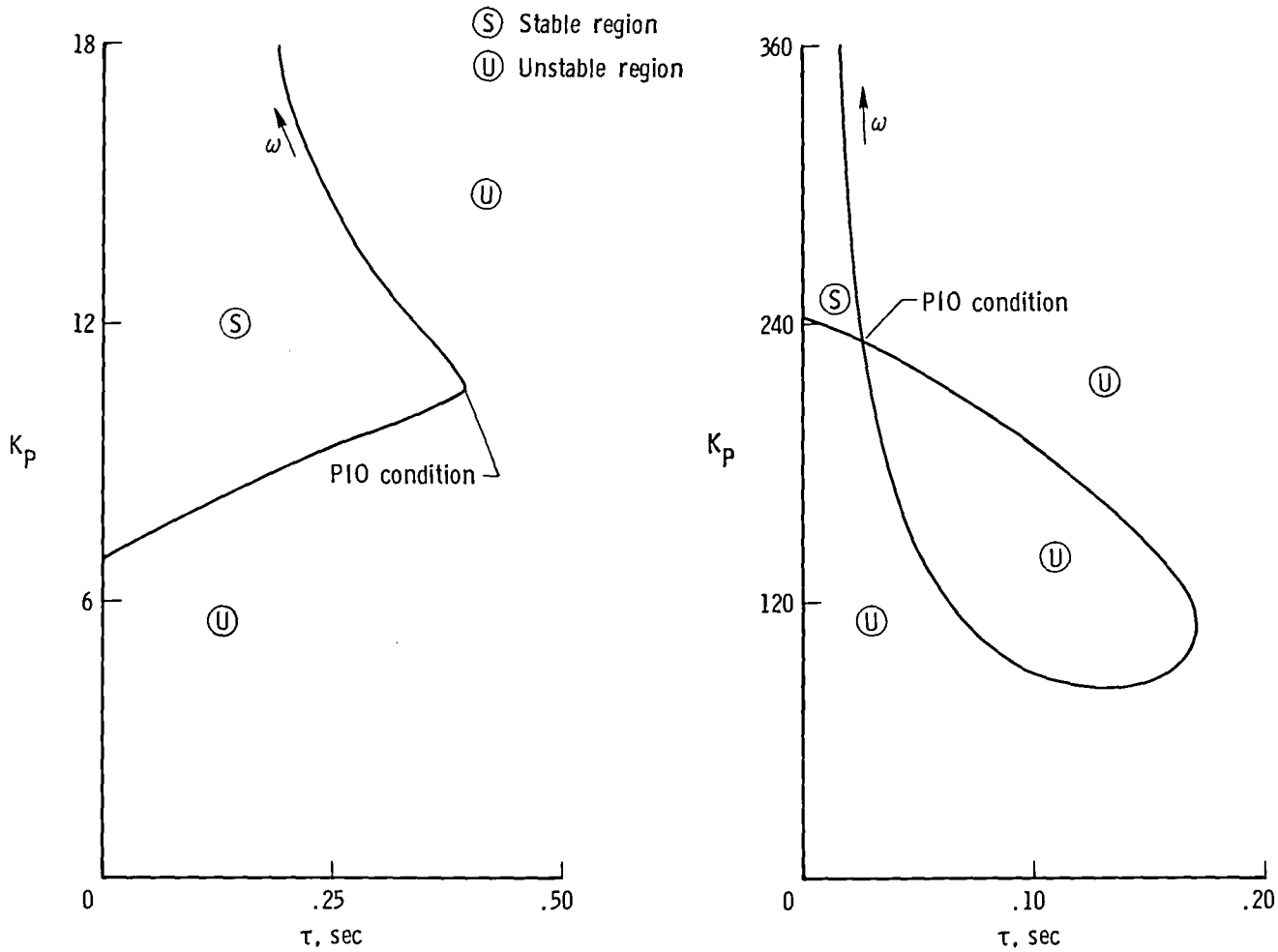


(a) $l_t$ = 91.44 m (300 ft).

(b) $l_t$ = 30.48 m (100 ft).

Figure 4.- Parameter-plane sketches for basic case at two different ranges.

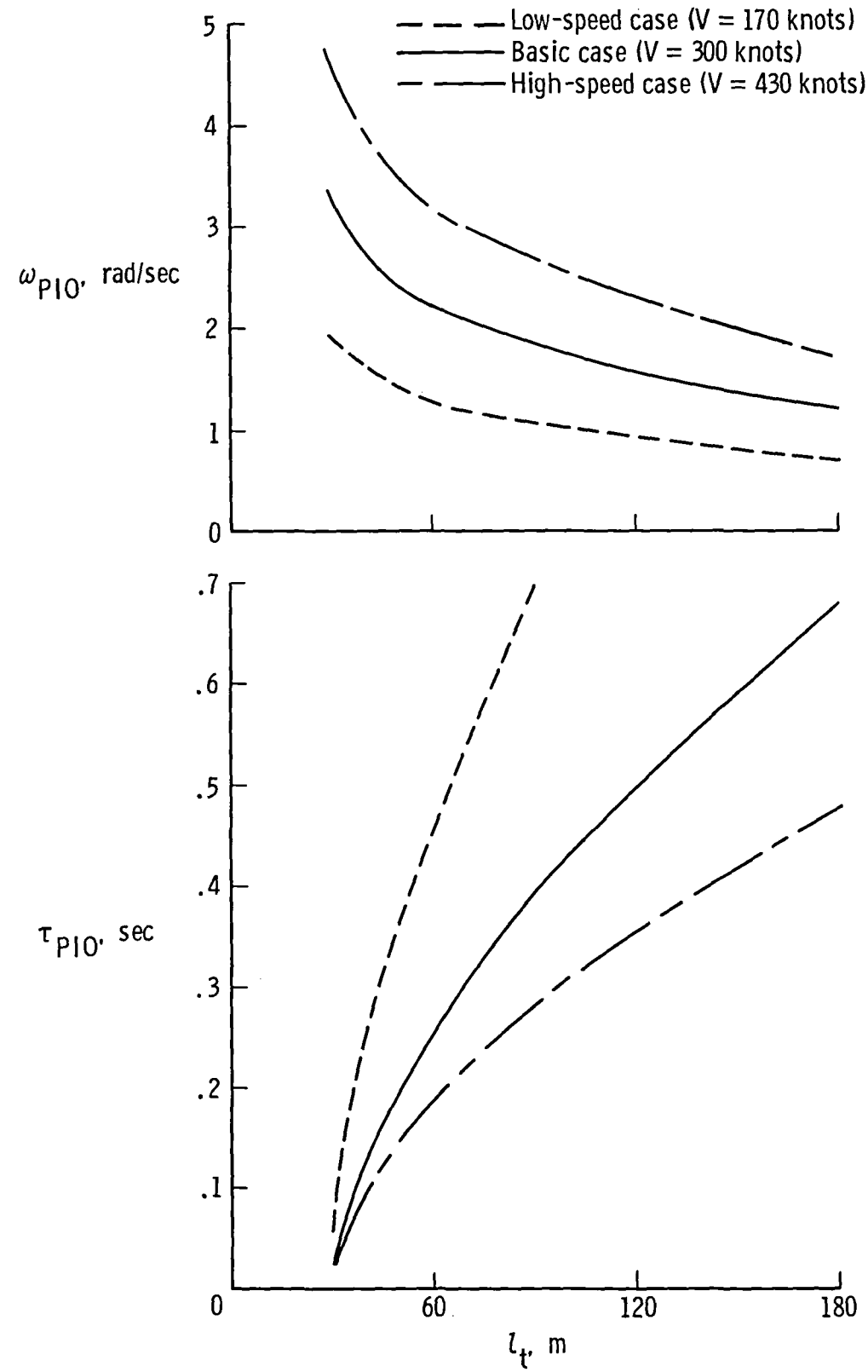


Figure 5.- Calculated effect of range and handling qualities on PIO conditions of frequency $\omega_{PIO}$ and time delay $\tau_{PIO}$ (basic, low-speed, and high-speed cases).

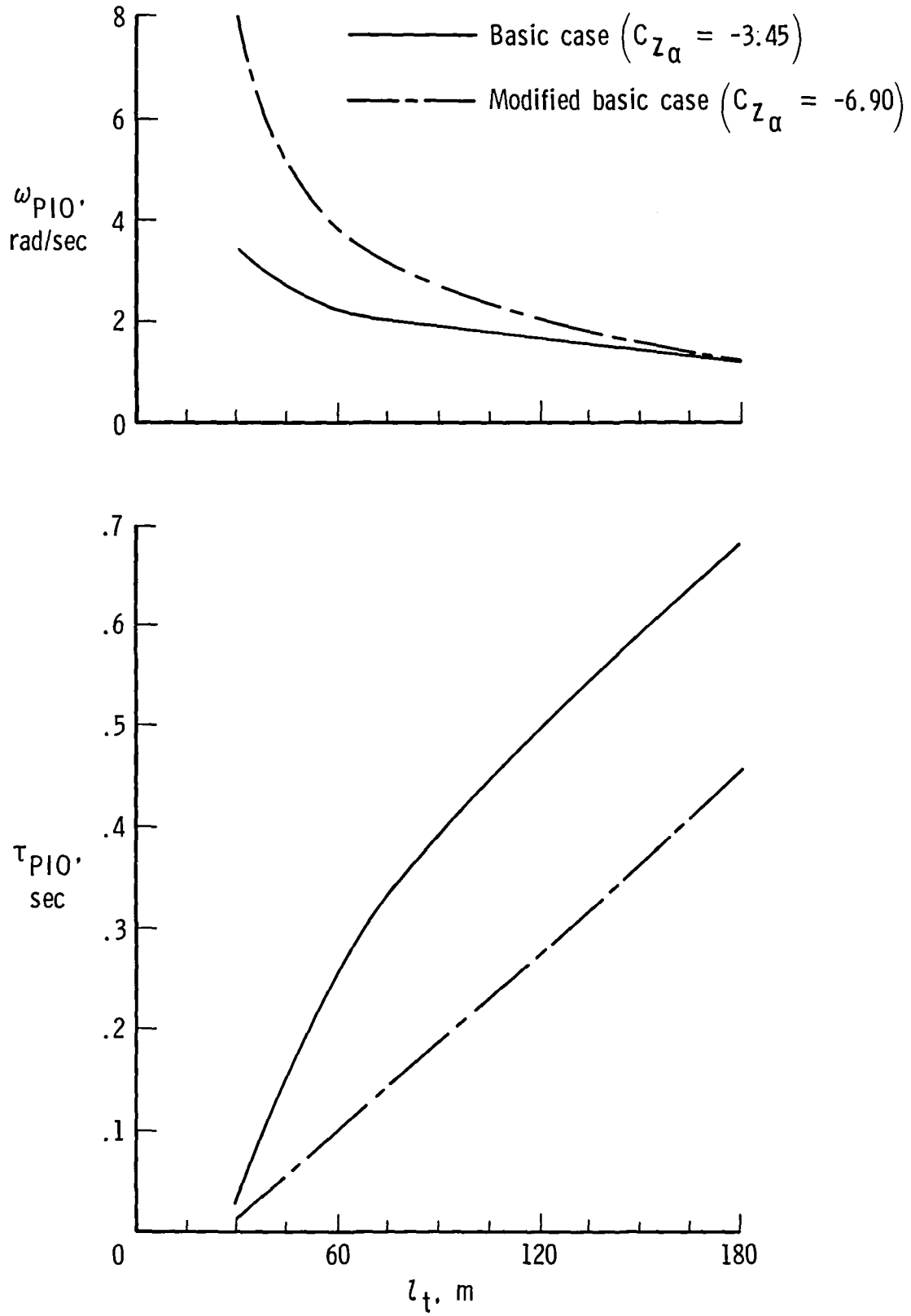


Figure 6.- Calculated effect of range and handling qualities on PIO conditions of frequency $\omega_{PIO}$ and time delay $\tau_{PIO}$ (basic and modified basic cases).

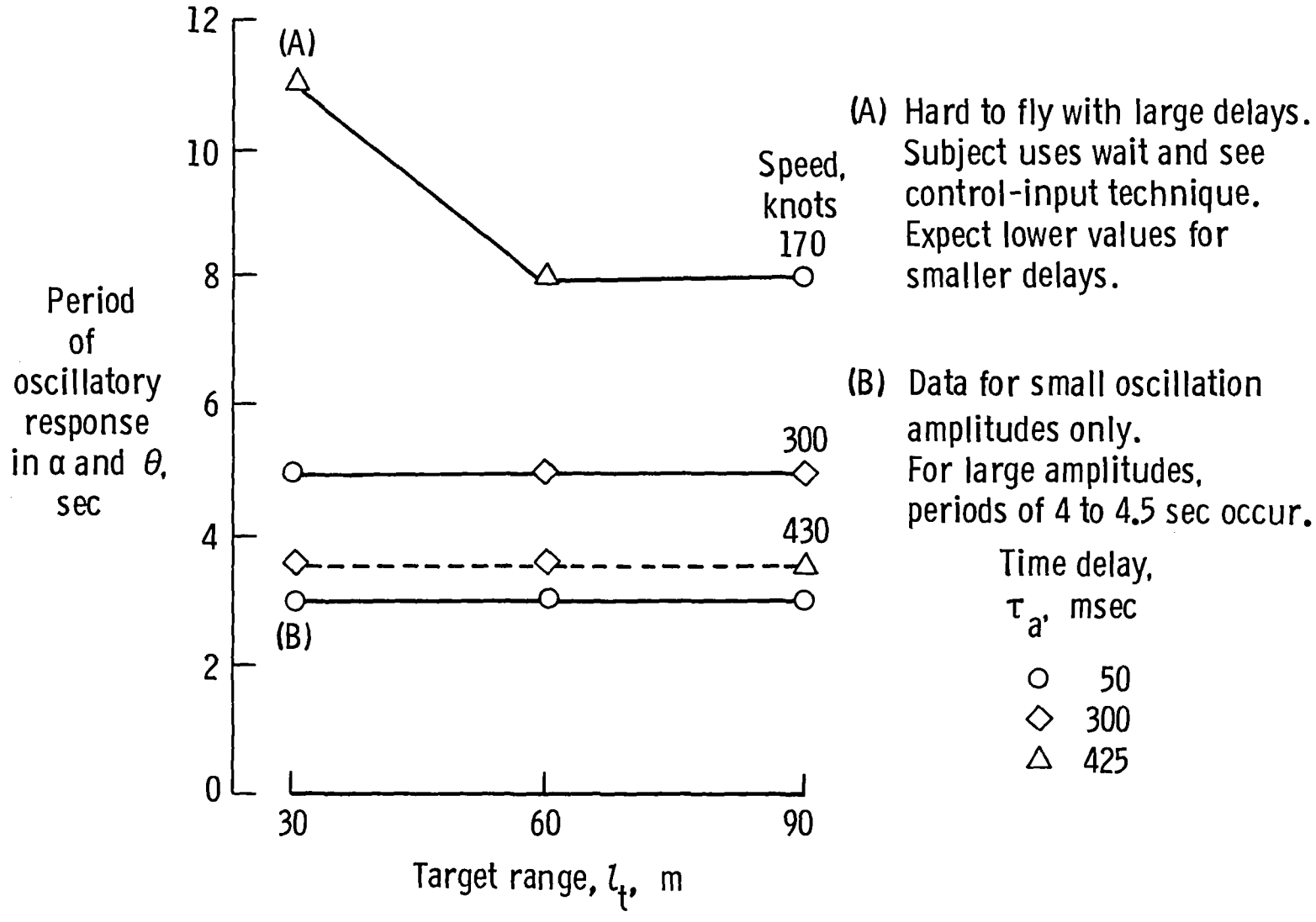


Figure 7.- Simulation results for the effect of range and speed on longitudinal oscillatory response.

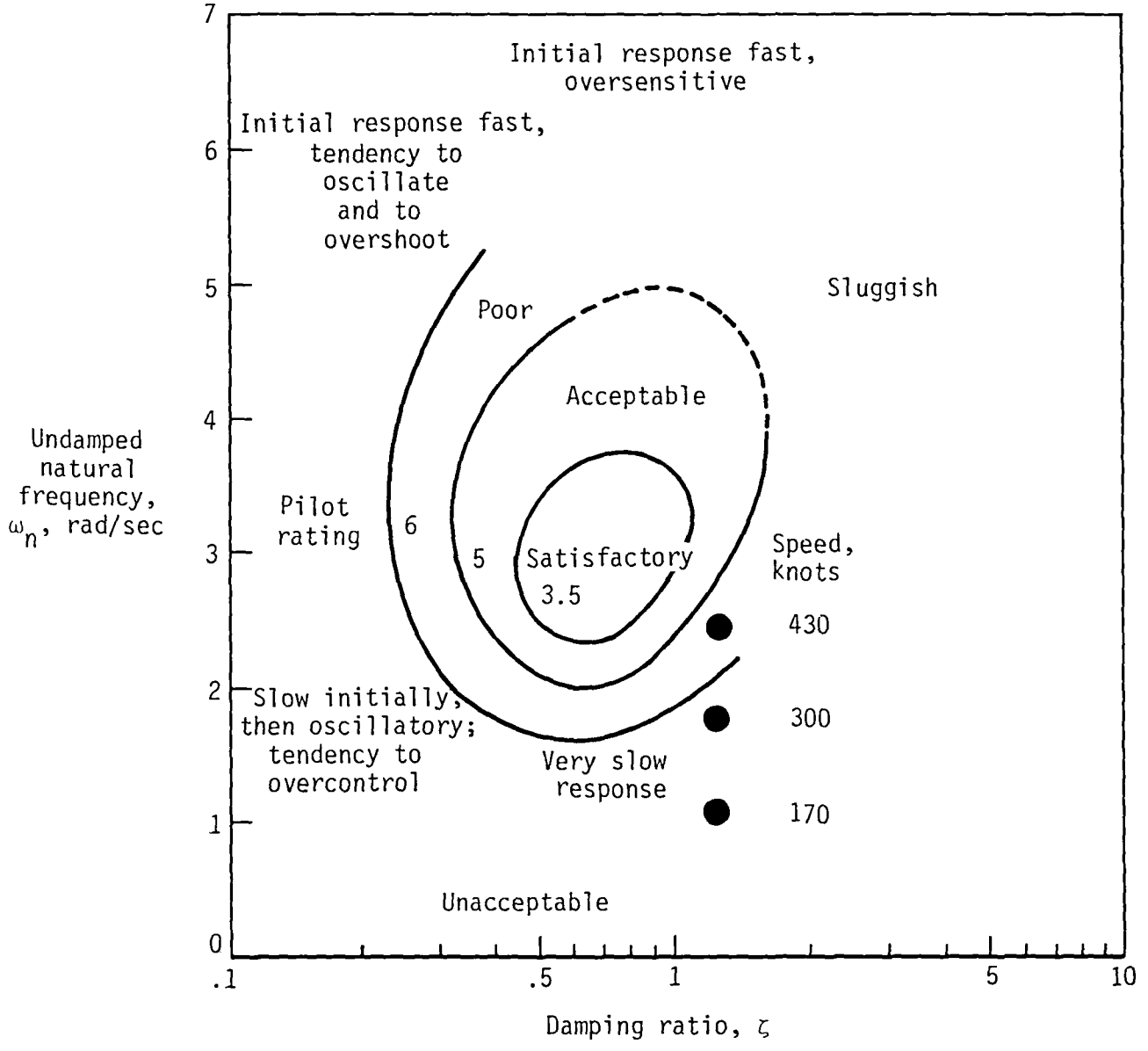


Figure 8.- Effect of changing orbiter speed on handling qualities as shown on the longitudinal short-period handling qualities chart from reference 8.

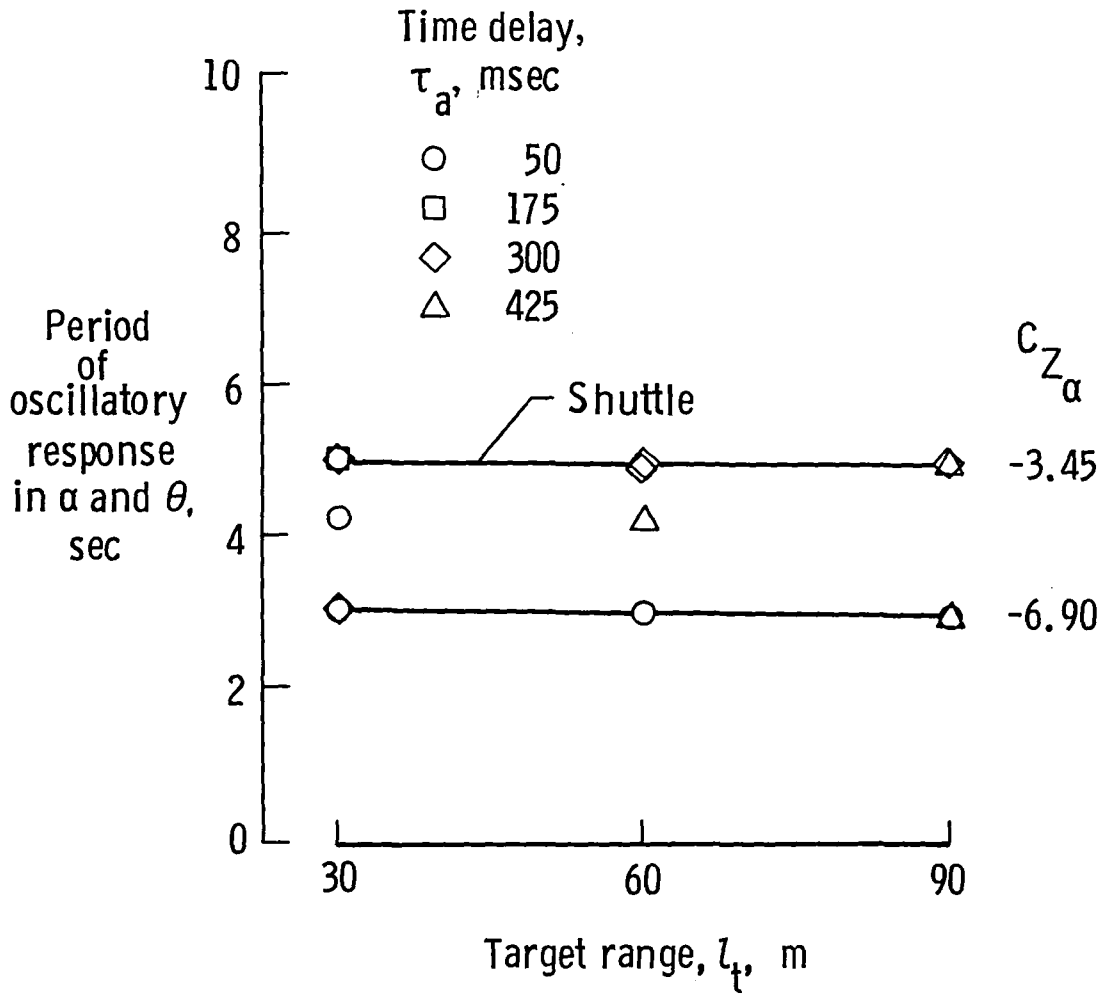


Figure 9.- Simulation results for the effect of $C_{Z_\alpha}$ on longitudinal oscillatory response.

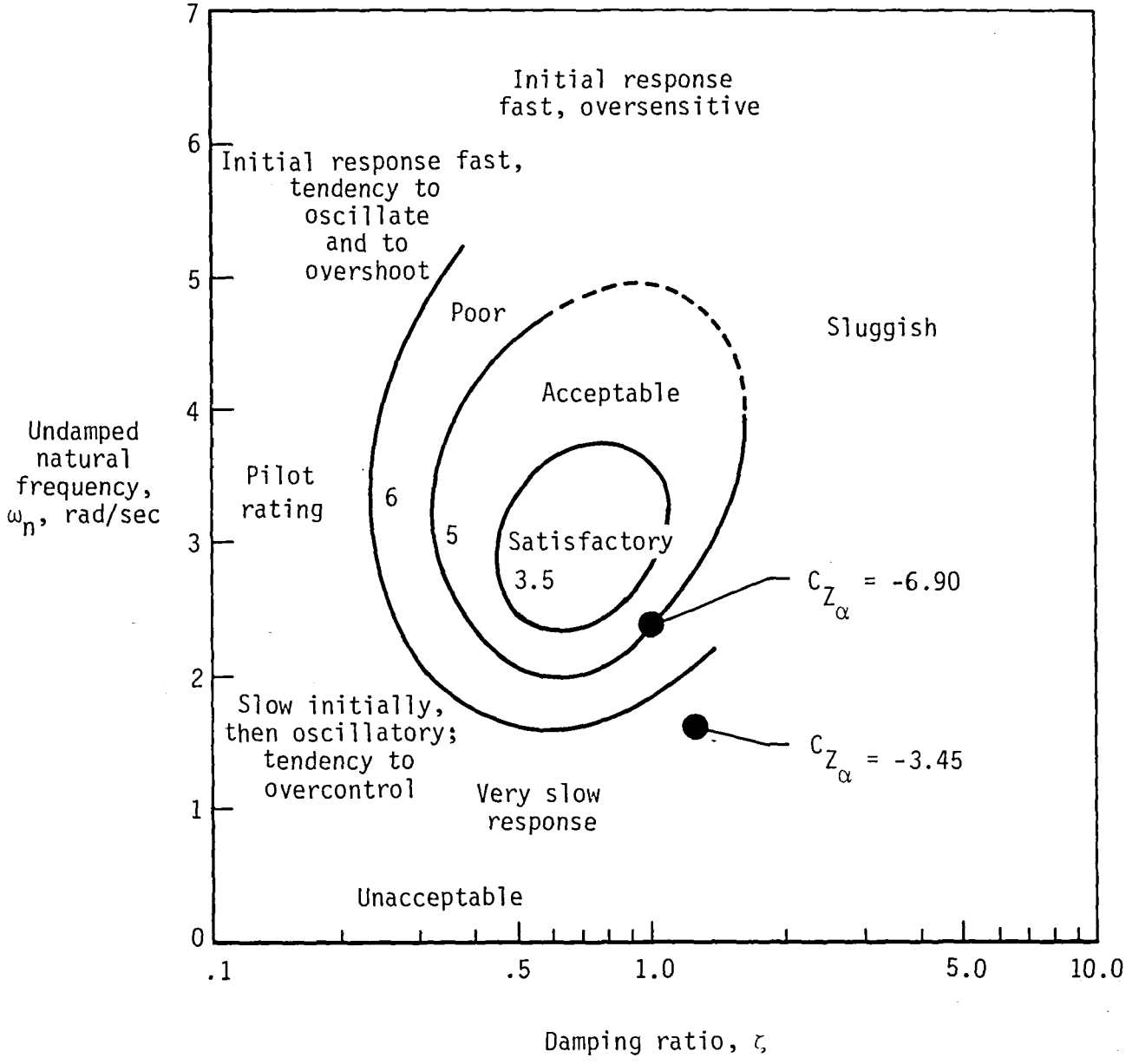


Figure 10.- Effect of changing $C_{Z_\alpha}$ on handling qualities as shown in the longitudinal short-period handling qualities chart from reference 8.

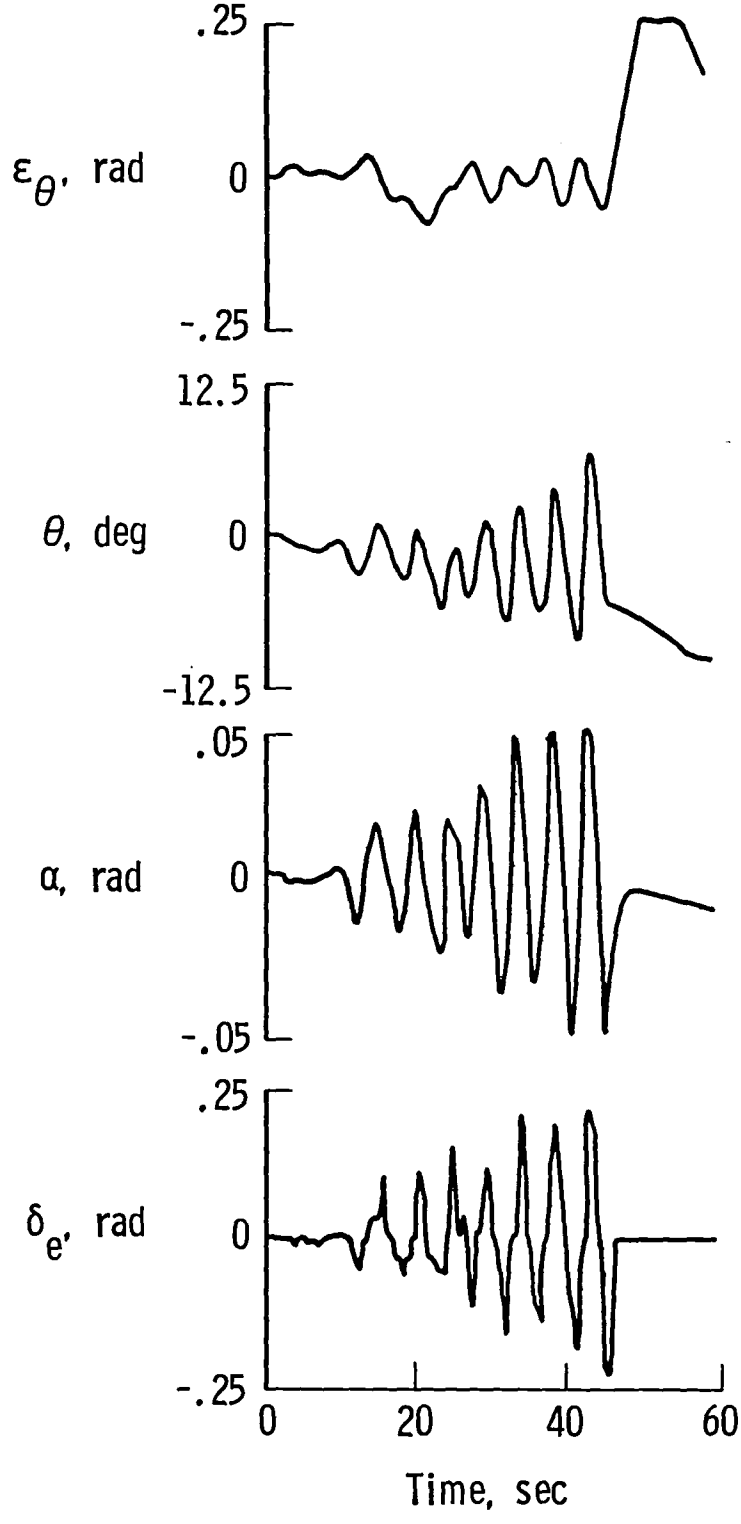


Figure 11.- Time history with V = 300 knots, $\iota_t$ = 60.96 m (200 ft), and $\tau_a$ = 300 msec.

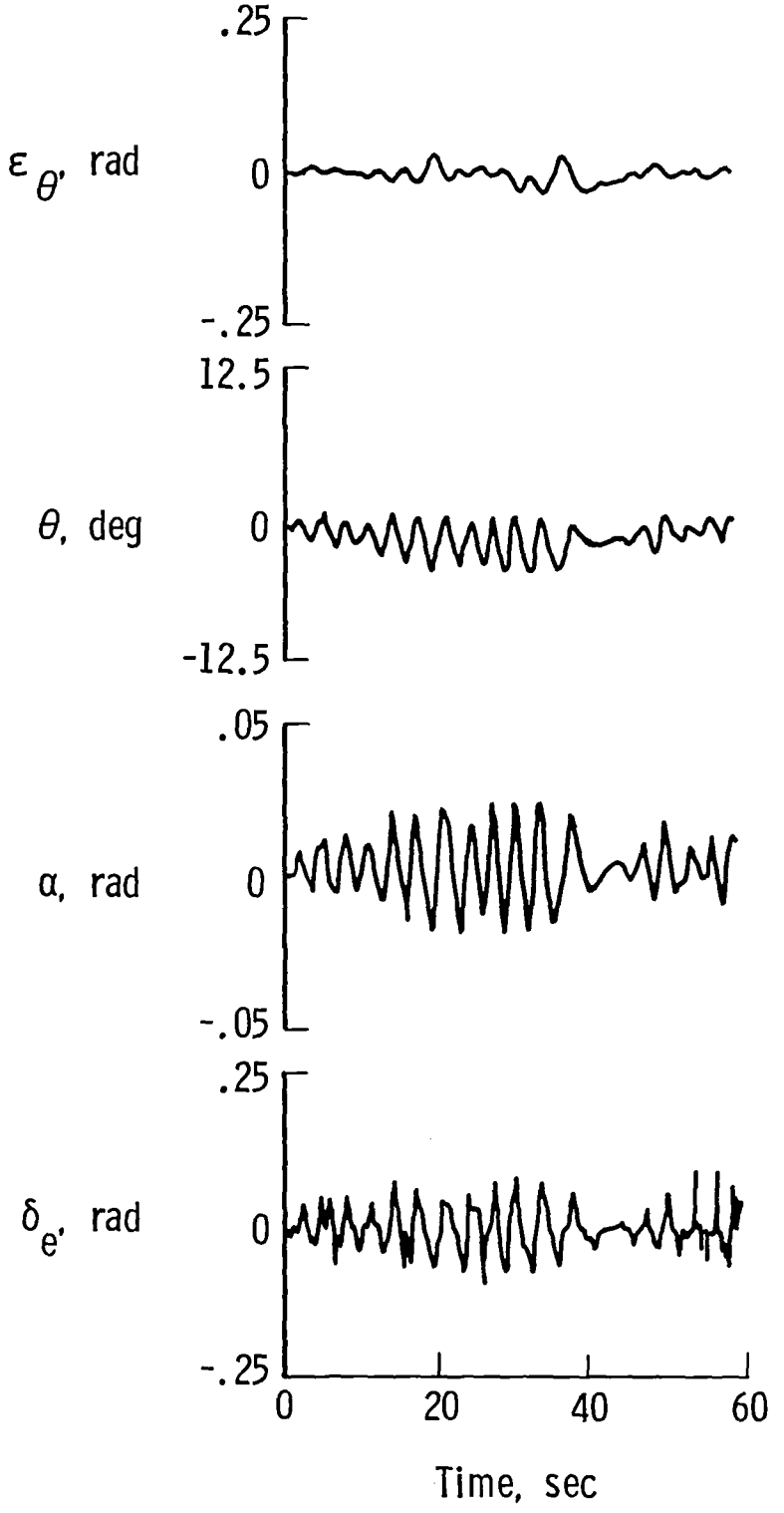


Figure 12.- Time history with V = 430 knots, $\iota_t$ = 60.96 m (200 ft), and $\tau_a$ = 50 msec.

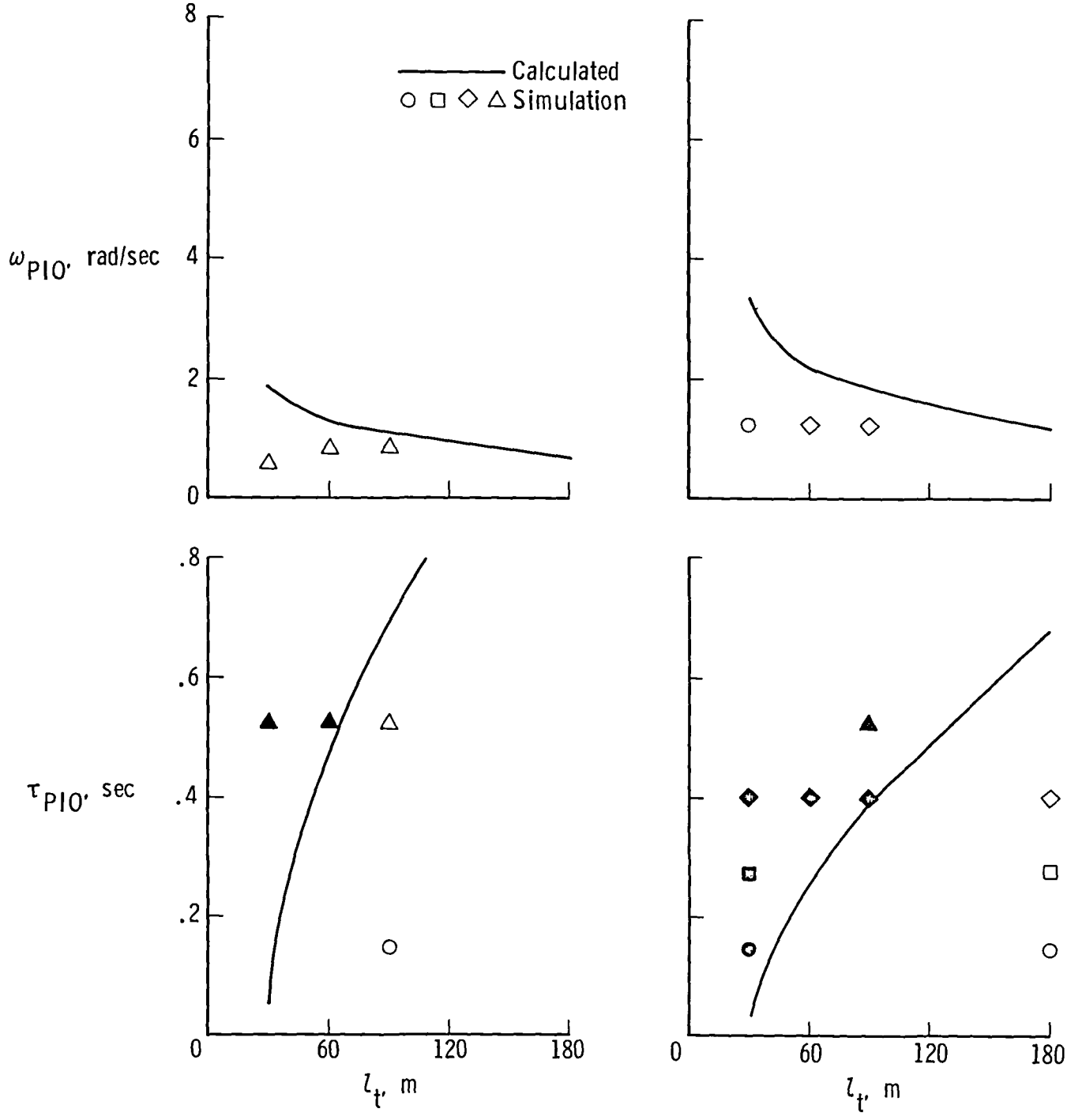


(a) Low-speed case.

(b) Basic case.

Figure 13.- Comparison of analytical predictions and experimental results. Shaded symbols indicated PIO occurred.

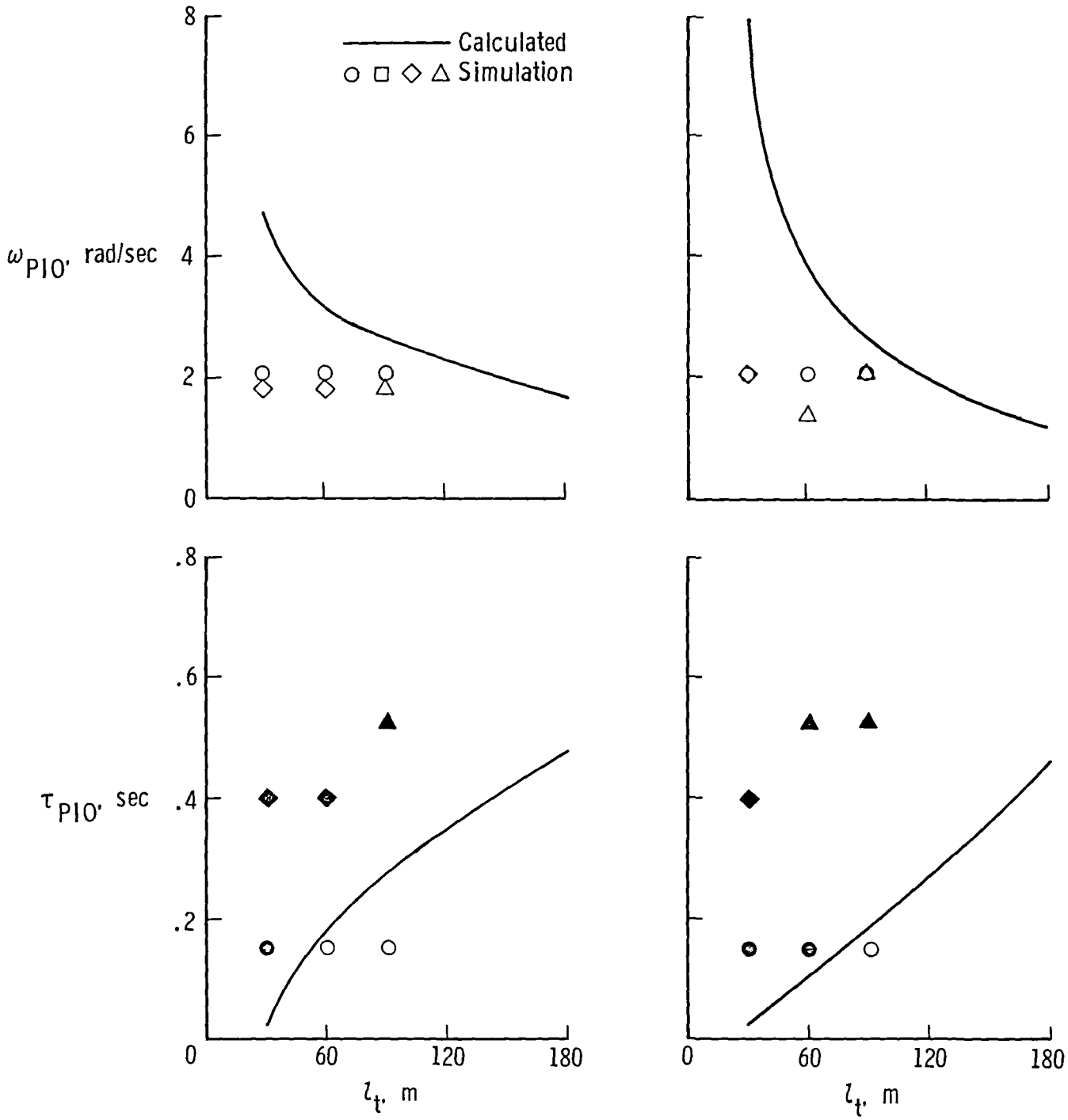


(c) High-speed case.

(d) Modified basic case.

Figure 13.- Concluded.

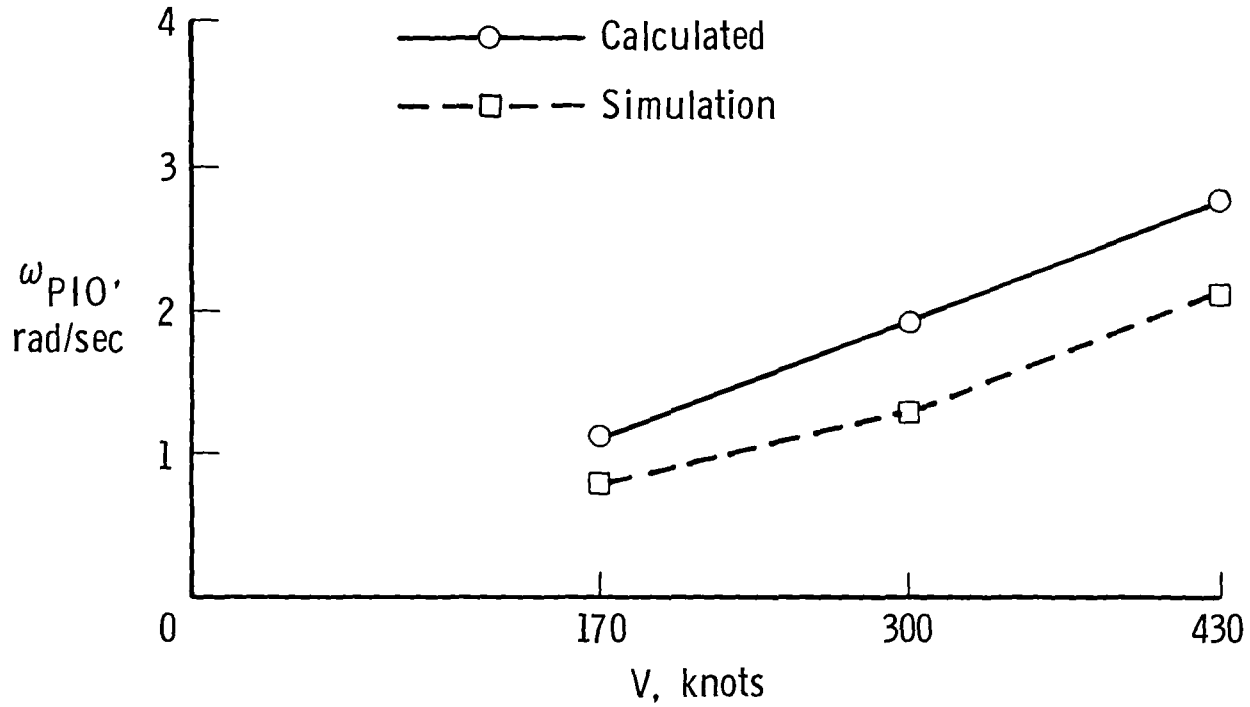


(a) Effect of speed (handling qualities).

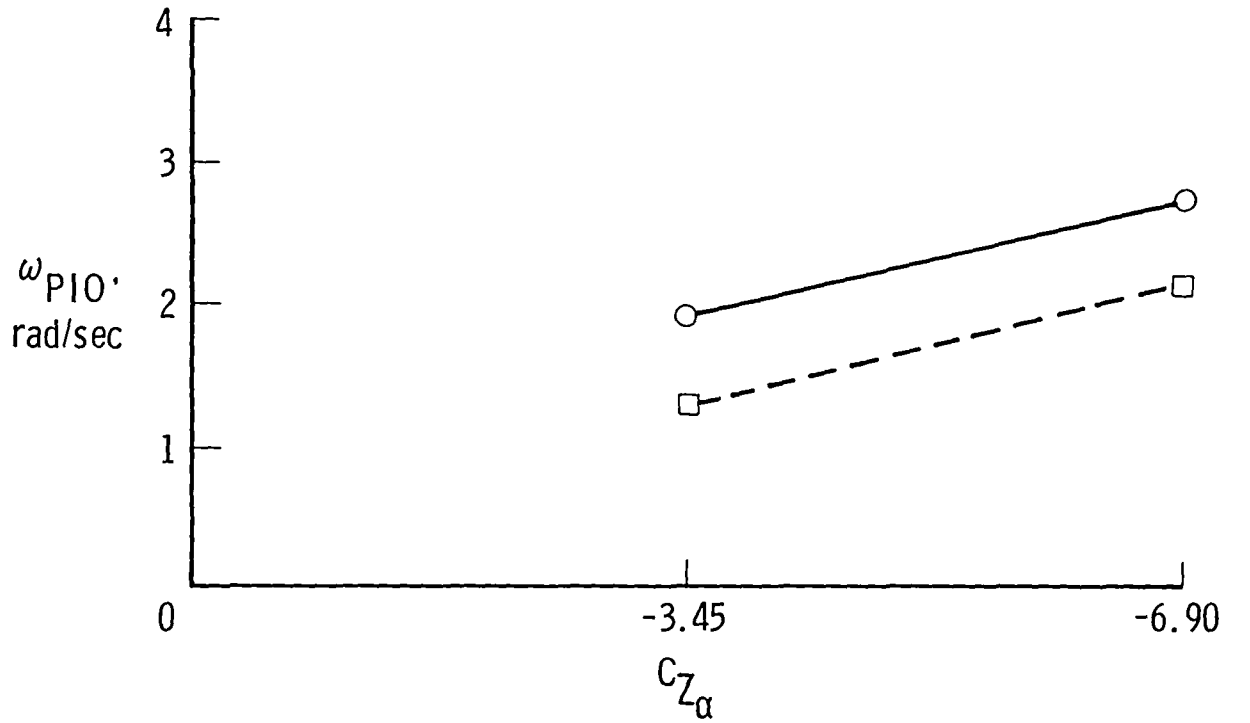


(b) Effect of stability derivative $C_{Z_\alpha}$ (handling qualities).

Figure 14.- Comparison of analytical predictions and experimental results indicating the effect of handling qualities on PIO frequency for a range $l_t$ of 91.44 m (300 ft).

| 1. Report No. | 2. Government Accession No. | 3. Recipient's Catalog No. |
|---|---|---|
| NASA TM-83267 | | |

| 4. Title and Subtitle | 5. Report Date |
|---|---|
| COMPARISON OF ANALYTICAL PREDICTIONS OF LONGITUDINAL SHORT-PERIOD PILOT-INDUCED OSCILLATIONS WITH RESULTS FROM A SIMULATION STUDY OF THE SPACE SHUTTLE ORBITER | April 1982 |
| | 6. Performing Organization Code: 505-34-33-06 |

| 7. Author(s) | 8. Performing Organization Report No. |
|---|---|
| Donald R. Riley and G. Kimball Miller, Jr. | L-14847 |
| | 10. Work Unit No. |

| 9. Performing Organization Name and Address | 11. Contract or Grant No. |
|---|---|
| NASA Langley Research Center<br>Hampton, VA 23665 | |
| | 13. Type of Report and Period Covered: Technical Memorandum |

| 12. Sponsoring Agency Name and Address | 14. Sponsoring Agency Code |
|---|---|
| National Aeronautics and Space Administration<br>Washington, DC 20546 | |

15. Supplementary Notes

16. Abstract

An analytical analysis of conditions producing pilot induced oscillations (PIO's) was made for the Space Shuttle orbiter in a landing-approach configuration for the task of nulling the elevation angle of the line of sight to a target vehicle. The analysis yielded a value of PIO frequency and a value for the amount of total-system time delay (pilot + control system) that can be tolerated before instability results. Calculations were performed showing the effect of varying the range to the target and of varying the handling qualities of the orbiter vehicle. Analytical predictions were compared with simulation results obtained using the Langley Visual/Motion Simulator.

| 17. Key Words (Suggested by Author(s)) | 18. Distribution Statement |
|---|---|
| Transport delays<br>Shuttle simulation<br>Pilot-induced oscillations | Unclassified - Unlimited<br><br>Subject Category 05 |

| 19. Security Classif. (of this report) | 20. Security Classif. (of this page) | 21. No. of Pages | 22. Price |
|---|---|---|---|
| Unclassified | Unclassified | 41 | A03 |

For sale by the National Technical Information Service, Springfield, Virginia 22161

NASA-Langley, 1982

National Aeronautics and
Space Administration

Washington, D.C.
20546

Official Business
Penalty for Private Use, $300

THIRD-CLASS BULK RATE

Postage and Fees Paid
National Aeronautics and
Space Administration
NASA-451



POSTMASTER: If Undeliverable (Section 158 Postal Manual) Do Not Return